

NBSIR 87-3586

The Wind Tunnel Model Surface Gauge for Measuring Roughness

T. V. Vorburger, D. E. Gilsinn, E. C. Teague,
C. H. W. Giauque, F. E. Scire, and L. X. Cao*

U.S. DEPARTMENT OF COMMERCE
National Bureau of Standards
Center for Manufacturing Engineering
Gaithersburg, MD 20899

June 1987

*Permanent Address: Department of Aircraft Manufacturing Engineering,
Northwestern Polytechnical University, Xian, China



U.S. DEPARTMENT OF COMMERCE

NATIONAL BUREAU OF STANDARDS

QC
100
.U56
87-3586
1987
C.2



00100
456
87-3536
1987
C.2

NBSIR 87-3586

**THE WIND TUNNEL MODEL SURFACE
GAUGE FOR MEASURING ROUGHNESS**

T. V. Vorburger, D. E. Gilsinn, E. C. Teague,
C. H. W. Giauque, F. E. Scire, and L. X. Cao*

U.S. DEPARTMENT OF COMMERCE
National Bureau of Standards
Center for Manufacturing Engineering
Gaithersburg, MD 20899

June 1987

*Permanent Address: Department of Aircraft Manufacturing Engineering,
Northwestern Polytechnical University, Xian, China

U.S. DEPARTMENT OF COMMERCE, Malcolm Baldrige, *Secretary*
NATIONAL BUREAU OF STANDARDS, Ernest Ambler, *Director*

Abstract

This report covers research performed in the optical inspection of surface roughness by members of the Center for Manufacturing Engineering under contracts L-4718B and L-20078B with the NASA Langley Research Center. The project has proceeded along two lines: first, research into a quantitative understanding of light scattering from metal surfaces and into the appropriate models to describe the surfaces themselves, and second, the development of a practical instrument for the measurement of rms roughness of high performance wind tunnel models with smooth finishes. The research has been discussed in previous articles and is only summarized here. This report is concerned primarily with the latter subject. We have developed a practical technique for the optical estimation of rms roughness based on three things: a commercially available, optical roughness gauge, a special nosepiece that allows for rapid alignment of the gauge on curved surfaces, and a series of comparator studies that correlate the results for S_N obtained by the gauge with rms roughness (R_q) measurements of surfaces by stylus techniques. S_N is an optical scattering parameter that is proportional to the variance of the light scattering angular distribution about its mean angle. We have proposed upper limit criteria for the value of S_N that should be expected on a properly finished model surface having rms roughness less than $0.2 \mu\text{m}$. We have estimated that valid measurements of S_N may be taken within an angle of 60° from the leading edge of the wind-tunnel model wing that we tested and have shown from stylus measurements that the roughness increases dramatically around the leading edge.

Key Words: aircraft, finish, light scattering, model, optical roughness, optical scattering, rms roughness, roughness, stylus, surface, transonic, wind tunnel

TABLE OF CONTENTS

	<u>Page</u>
1. Introduction	1
2. Description and Use of the Model Surface Gauge	3
3. Experimental Tests of the Model Surface Gauge.	11
4. Limitations of the Present Instrument	38
5. Related Work	39
6. Acknowledgments	43
7. References	44
Appendix A	46

1. Introduction

In the fall of 1980, NASA and NBS initiated a project, with partial funding from NASA under contracts L-4718B and L-20078B, to address any potential new problems that might be imposed on the surface finish requirements for models to be used in the National Transonic Facility, a high-pressure, cryogenic wind tunnel under development at the time and since completed. At the largest Reynolds numbers that the National Transonic Facility would achieve, admissible roughness heights for the surfaces of models fell below the surface finishes currently specified for models. These higher demands for surface finishes of the models arose because surface roughness influences skin friction, shock wave location, and boundary layer separation location. Generally the aim in fabricating a model's surface is to make it smooth enough that it does not produce a measurable aerodynamic effect. Estimated roughness heights at which surface irregularities can have an aerodynamic effect at typical Reynolds numbers in the NTF are 0.25 micrometers (10 microinches) or higher [1].

The objectives of the joint NASA/NBS project were therefore: (1) to evaluate the performance of stylus instruments for measuring the topography of NTF model surfaces both for monitoring during fabrication and as an absolute measurement of topography, (2) to measure and characterize the true 3D topography of NTF model surfaces so that their characteristics could be related back to that of sand grain surfaces historically used to obtain data on surface roughness versus drag, and (3) to develop a prototype light scattering instrument that would allow for rapid assessment of the surface finish of a model surface.

Work to accomplish the first objective has consisted of comparing research grade and shop grade stylus measurements of the surface finish of three test specimens fabricated by NASA [1]. We concluded from this study that the shop grade instruments can damage the surfaces of models and that their use for monitoring fabrication procedures can lead to surface finishes, in critical areas of the leading edges of wings, that are substantially out of range.

To accomplish the second objective, NBS has developed a 3D stylus instrument [2]. This instrument enables one to obtain quantitative images of surface topography with a lateral resolution of less than 1 micrometer and vertical resolutions of less than 1 nm. A research grade stylus transducer is incorporated into the instrument so the stylus forces are usually 20 mg or less. This experimental capability has been used to measure the 3D surface

microtopography of NTF model components and metal surfaces prepared with the same processes used to finish model surfaces. While this characterization work is continuing, some data for model surfaces has been described in earlier work [1,2].

Based on discussions with NASA personnel concerning the third objective, the measurement technique developed should: (1) be capable of detecting and quantifying surface topography variations for surface roughnesses less than about 0.25 micrometers, (2) be usable during model fabrication on surfaces that have radii of curvature 2.5 mm or larger, (3) provide characterizations of the surface topography which are sufficient to give feedback to a fabricator for optimizing model surfaces, and (4) provide characterizations such that surfaces produced by different processes can be compared and qualified in a consistent manner.

The model surface gauge (MSG) described in this report is a step towards satisfying the third objective. The recommendations concerning its use that are given in this report address the first three of the criteria for an instrument to assess the finish of a model surface. In addition, the MSG is easy to use and align and is therefore capable of rapidly sampling the surface roughness in a number of places on the models. Other technical papers [3-8] describing experimental and theoretical outputs of this joint NASA/NBS project contain adequate information for the development of an instrument that could meet the fourth criterion. Development of a practical shop instrument capable of discriminating between surfaces produced by different processes was beyond the scope of this project.

During the course of this project, several research questions have arisen which are the subject of ongoing work on measurement techniques and their applicability to aerodynamic surfaces. First, in interpreting and generalizing the classical work of Nikuradse [9], what properties of the surface topography influence the air flow pattern across a surface and what are the admissible values for these as a function of Reynolds number? A closely related issue concerns the statistical characterization of irregularity heights and irregularity spacings that are most applicable. Furthermore, the modeling of the three-dimensional aspects of light scattering from surfaces and its detailed relationship to the surface topography have only been treated in a preliminary way within the scope of this project and should be studied in more depth. Early results on this work were recently reported [8].

Section 2 gives a description of the MSG design and its operating principles. Section 3 describes the experimental tests to relate the optical roughness values to the standard rms roughness values measured by a stylus instrument and the tests to determine the conditions for proper operation of the instrument. Section 4 outlines precautions about using the MSG and about the data in Section 3, and Section 5 gives some more details about related work described earlier in this Section.

2. Description and Use of the Model Surface Gauge

The MSG inspects surface roughness by measuring the angular distribution of light scattered from the surface. It consists of a commercial Rodenstock RM 400 instrument* modified with a special delrin nosepiece. The purpose of the nosepiece is to allow the gauge to be gently rested on the surface of the model without damaging it and in such a way that valid readings may be taken of the angular distribution from the curved surface.

A schematic diagram of the optical system is shown in Fig. 1 [10]. The source consists of a light emitting diode (LED) that produces radiation at a near infrared wavelength of 800 nm. This radiation passes first through a collimating lens, then through one side of a special measuring lens, that focuses and redirects the radiation so that it illuminates the surface to be measured at a slight angle but very close to the optical axis. The radiation scattered by the surface then passes through the other side of the measuring lens and is redirected to a linear photodiode array which measures a line sample of the scattering light beam to obtain an angular distribution of light intensity.

If the surface is smooth, the pattern of scattered light falling on the diode array is nearly the same as the circular pattern of the incident beam leaving the collimating lens. If the surface is rough, the scattered radiation pattern is broadened. When the pattern of marks (lay) left on the surface by the finishing process is unidirectional, the scattered radiation pattern is elongated along the roughness direction. All of the NASA specimens were

* Certain commercial equipment are identified in this report to specify adequately the experimental procedure. In no case does such identification imply recommendation or endorsement by the National Bureau of Standards, nor does it imply that the equipment identified is necessarily the best available for the purpose.

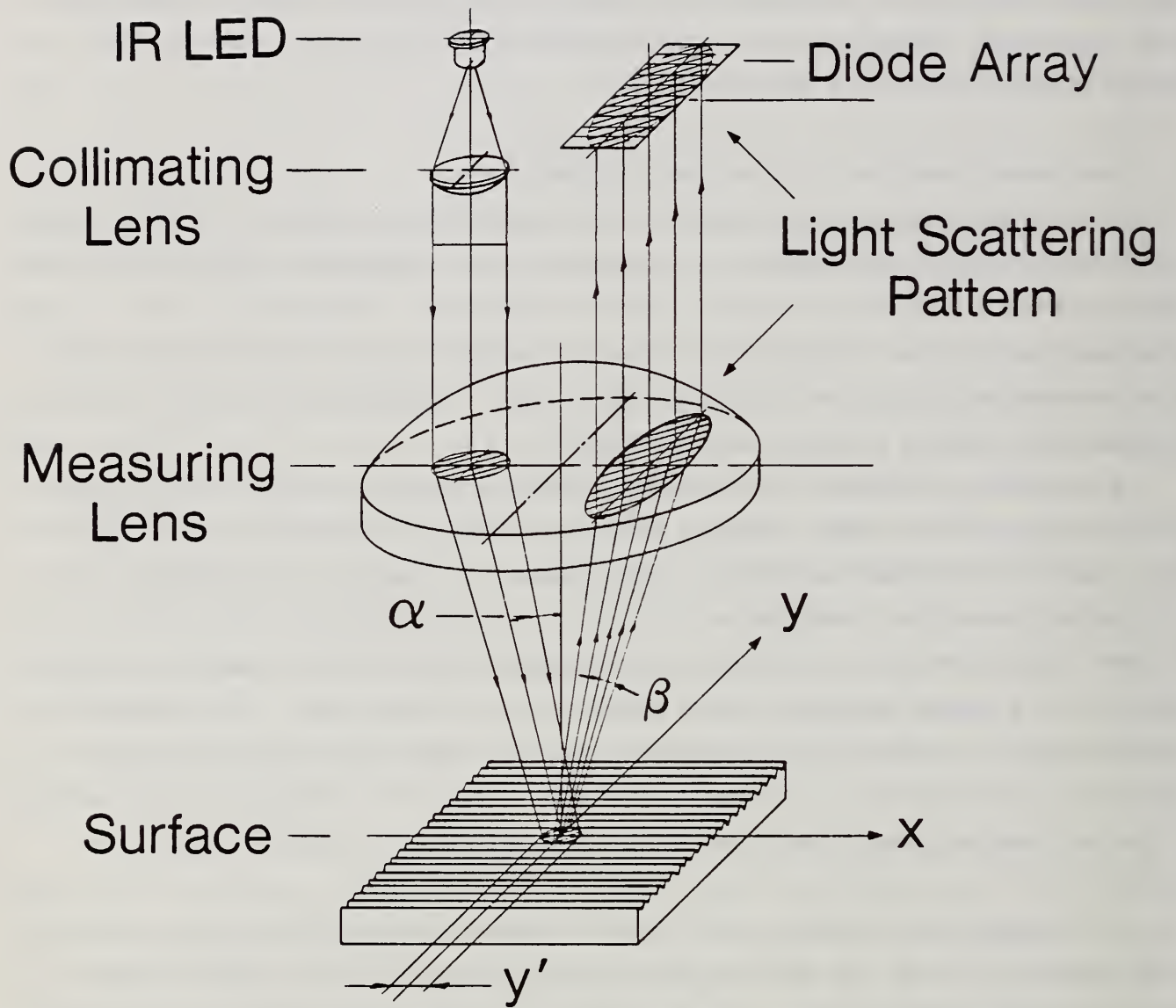


Figure 1 Schematic diagram of the optical system of the MSG (taken from Reference 10).

finished by unidirectional hand lapping and hence yield elongated scattering patterns. Figure 1 shows the MSG with the proper rotational alignment for sensing the unidirectional surface roughness since the long axis of the array is parallel to the elongated scattering pattern.

Important parameters of the optical system are the angle of incidence of the light (α), the angular resolution and angular range (β) of the detected scattering pattern, the illumination spot size y' , and the axial distance of the surface from the measuring lens. The instrument supplied to NASA has an angle of incidence of about 8.4° [10]. The angular range of the detector is $\pm 15^\circ$ about the center. It is determined by the length of the diode array and the focal length of the measuring lens. The axial position of the surface is not a critical factor because the system has been designed to be insensitive to misalignment in the axial direction [10]. The tolerance in axial positioning is ± 2 mm.

The gauge outputs a light scattering parameter called S_N that serves as a measure of surface roughness condition. The unitless parameter S_N is proportional to the variance of the light scattering distribution about the mean (M) of the data. Figure 2 shows a typical bell-shaped, light-scattering distribution as measured by the gauge. The distribution is composed of 20 diode readings identified as $i = 1, 2, \dots, 20$ with intensity values I_i . The mean value M of the distribution with respect to the center of the array is then given by

$$M = (1/I_s) \sum_{i=1}^{20} I_i \cdot (i - 10.5), \quad (1)$$

where I_s is the sum of the 20 intensity values of the array and the center of the 20-diode array is halfway between the tenth and eleventh diodes ($i = 10.5$). The light scatter parameter S_N is then given by

$$S_N = (\kappa/I_s) \sum_{i=1}^{20} I_i (i - 10.5 - M)^2, \quad (2)$$

where κ is a normalizing factor that yields an S_N value of 100 if all of the intensity values I_i are equal.

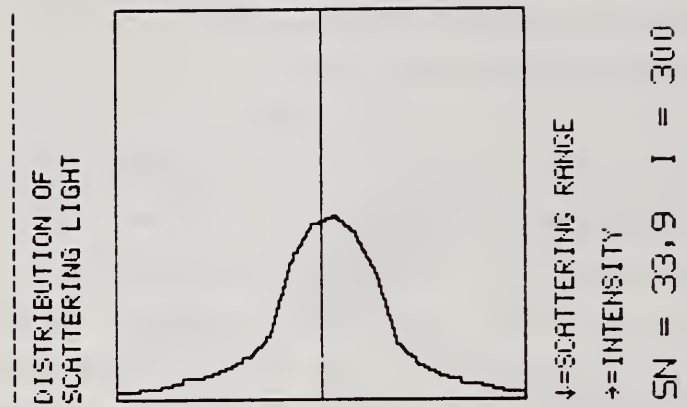


Figure 2 Typical light scattering distribution as measured and recorded by the MSG. The abscissa spans an angle of about $\pm 15^\circ$. The total intensity I and S_N values are also shown as part of the printed record. The mean value M is not printed, but is displayed on the instrument controller. The vertical line shown here is the ordinate axis.

In general, the value of S_N increases as the roughness of the surface increases. As shown in our other experimental and theoretical studies, the shape of the angular distribution is a complex function of roughness irregularity heights, height distributions, and spacings. All these properties cannot be boiled down to a single parameter. However, for a given type of surface, the one S_N parameter may be used to establish relative roughness heights. Therefore, we use the S_N value as a comparative estimator of the root mean square roughness R_q . In addition to S_N , the system also outputs the values of M and I .

Two calibration checks should be performed before using the MSG. The first is a procedure for nulling the dark current of each detector in the array. Normally this is accomplished by holding a special light absorbing cell over the nosepiece of the detector head and following the manufacturer's instructions for the nulling procedure. However, the special nosepiece to be described does not adapt to the light absorbing cell, and it is sufficient to perform the manufacturer's nulling procedure in a dark room.

Second, a check should be made of the gauge response for a smooth surface. To accomplish this, a small mirror or smooth glass plate may be held against the nosepiece. The angular distribution and S_N reading are then recorded and compared with results from the manufacturer's setup procedure. After this, the MSG is ready to use.

For a flat surface the gauge may be easily aligned to yield an appropriate S_N reading. This can be shown by referring to Fig. 3 and considering the three angular misalignment errors that can occur. If the gauge is misaligned by rotation about the x-axis, (Fig. 3a) the misalignment can be sensed and corrected by rotating the gauge so that $M = 0$. If rotation around the y-axis is the problem, the scattering pattern will move off the axis of the array (Fig. 3b) and will result in a value of total intensity I that is less than the maximum. Therefore, the gauge orientation around the y-axis can be manually corrected to yield a maximum value for I . Finally, if the gauge is misoriented by rotation around the z-axis, the radiation pattern falling on the diode array will appear to be narrower than it actually is (Fig. 3c). Hence, the gauge can be properly oriented by looking for a maximum S_N reading as it is rotated about the z-axis.

The nosepiece has been designed for manual operation on the curved surfaces of aerodynamic models. A photograph of the nosepiece is shown in Fig. 4, and a

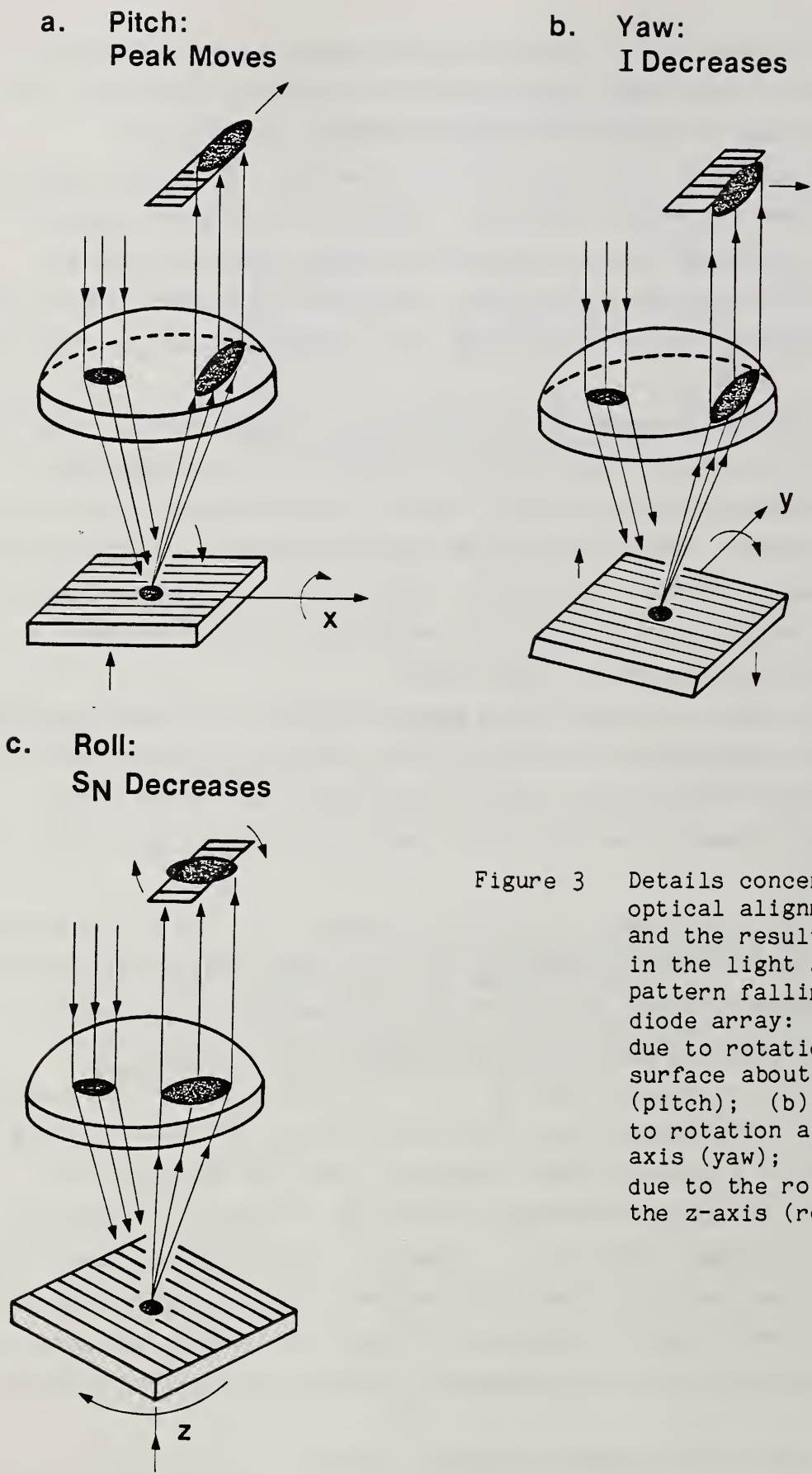


Figure 3 Details concerning the optical alignment errors and the resulting changes in the light scattering pattern falling on the diode array: (a) changes due to rotation of the surface about the x-axis (pitch); (b) changes due to rotation about the y-axis (yaw); (c) changes due to the rotation about the z-axis (roll).

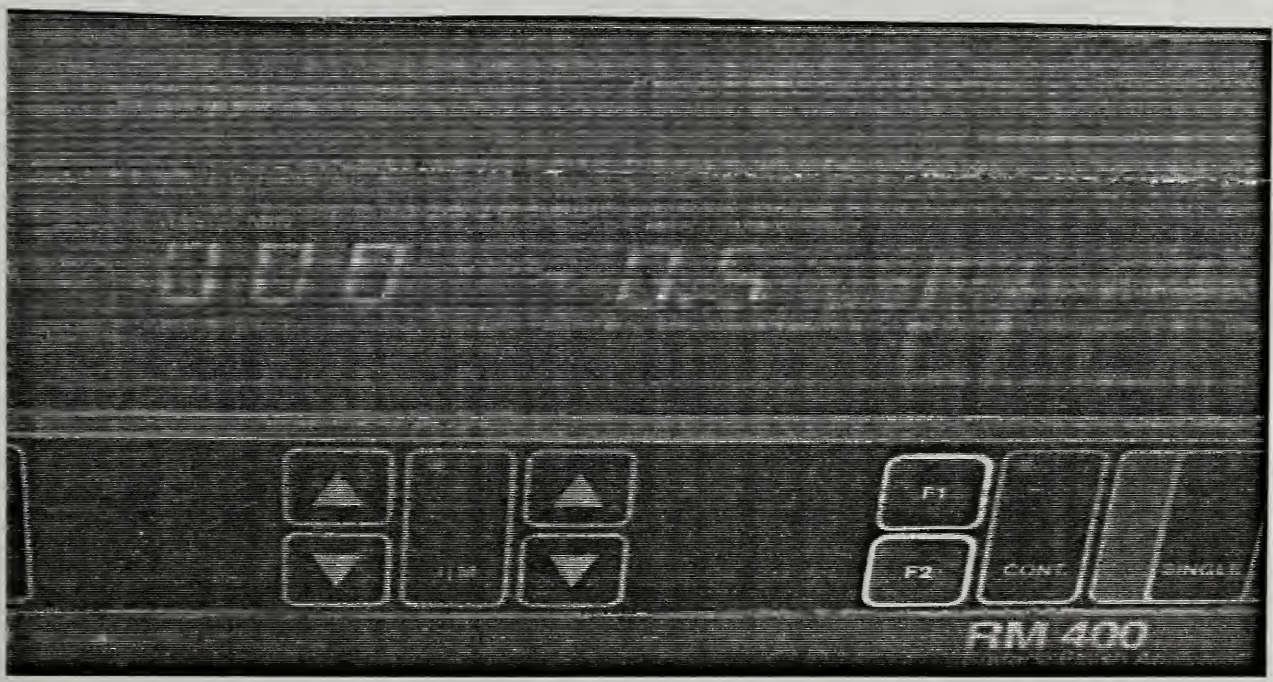
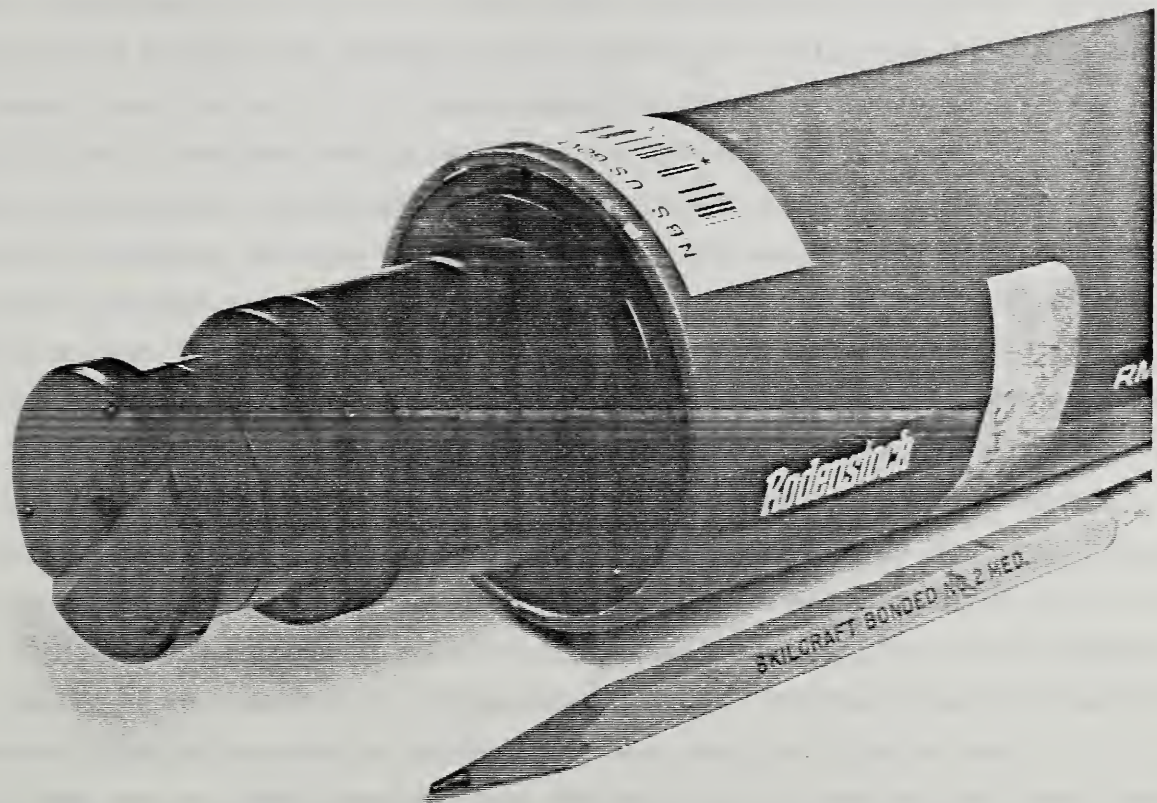


Figure 4 Photograph of the nosepiece mounted on the sensor head. The controller panel is shown below.

set of machine drawings is given as Appendix A. The nosepiece permits the operator to hold the gauge against the part so that it is constrained with good axial alignment and with close rotational alignment about the x and y axes (Fig. 3). The operator then rotates the gauge about the z-axis so that proper azimuthal orientation is achieved as indicated by the maximum value for S_N . As shown in Appendix A, the nosepiece contains a precision bearing that allows easy rotation. When the MSG is used to measure gently curving surfaces such as those on the top surface of a model airplane wing, the nosepiece contacts the surface at the three spherical points of support. On the other hand, when the MSG is used to measure highly curved surfaces near the leading edge of the wing, the v-groove of the nosepiece contacts the wing.

The recommended procedure for inspecting the roughness at a position on the model is to rest the nosepiece on the surface, contacting it by means of the three feet or the v-groove. Then, while holding the nosepiece steady, the gauge head should be rotated about its axis to produce a maximum S_N reading. This ensures that the elongated angular distribution from the surface is well aligned with the diode array. As discussed before, the elongated angular distribution comes from the unidirectional roughness lay pattern formed by the hand lapping finishing process along the direction of flow. That means that the MSG can also be used to determine the lay direction.

As the gauge is rotated, the maximum S_N reading and the total signal intensity (I) are then noted. The gauge should then be rotated approximately 180° until a second S_N maximum is found. S_N and its accompanying intensity value I are again noted. The final S_N reading is the one corresponding to the larger of the two I values. In accordance with considerations to be described in Sec. 3, this reading should be less than 50 for an acceptable surface. If the S_N reading is between 50 and 72, the surface roughness is marginal, and if the S_N reading is greater than 72, the surface roughness is likely unacceptable assuming that an acceptable wind tunnel model should have rms roughness R_q less than $0.20 \mu\text{m}$ ($8 \mu\text{in}$).

From our preliminary testing on the prototype instrument, it appears that valid readings may be taken on nearly all areas of the aerodynamic model wing except the most highly curved positions on the leading edge. There are two signal criteria from the gauge that indicate that it is being used on a proper location. First, the S_N value should give a clear maximum as the gauge is rotated through the angular position that intercepts the radiation pattern

caused by the unidirectional roughness marks. This position is easy to spot by eye and the adjustment is easy to perform after some experience with the gauge has been gained. Second, the total signal intensity I should be 50 or greater. This represents about 5% of the total intensity measured for a highly reflecting specular surface. The actual value depends on the LED intensity and the factory settings for sensitivity and varies from one unit to the next. The second criterion should ensure that the x and y angular alignment of the gauge with the surface is good enough so that a significant portion of the optical angular distribution is falling upon the diode array.

The surface roughness is a critical factor on the leading edges of model wings due to aerodynamic considerations. However, these areas are also more difficult to finish as well as to measure because of the high surface curvature. Therefore, it is important to know how close to the leading edge the gauge may be used. From our studies to be described in Sec. 3, we have developed the criterion that the gauge may be used to within about a 60° angle of the leading edge on both the upper and lower wing surfaces. Figure 5 shows a cross section of the leading edge. The angular direction normal to this edge is taken to be equal to 0° and various angular positions with respect to this origin are also shown. The numerical angular positions are equal to the slope angle of the surface with respect to its vertical slope angle at the leading edge. Hence the $+80^\circ$ position is located at the top of the wing's curved surface where the surface is nearly horizontal and the -80° position is at the bottom.

3. Experimental Tests of the Model Surface Gauge

The MSG was tested on 35 stainless steel surfaces with hand lapped finishes typical of high performance wind tunnel models. These surfaces included 11 flat specimens of different stainless steel materials having varying degrees of finish and 24 positions on a rear wing of a Pathfinder model. Table I describes the specimens and the wing positions, and Fig. 6 depicts the wing positions. The positions W-1, 2, and 3 are gently curving positions on the top surface of the wing. W-7, 8 and 9 are positions of increasing curvature near the leading edge. W-4 and 6 represent sets of positions around the leading edge of the wing at its wide end near the fuselage and at its tip respectively. At each of the W-4 and 6 locations, nine readings were made at various angles with respect to the 0° position at the leading edge itself. All of these surfaces were tested

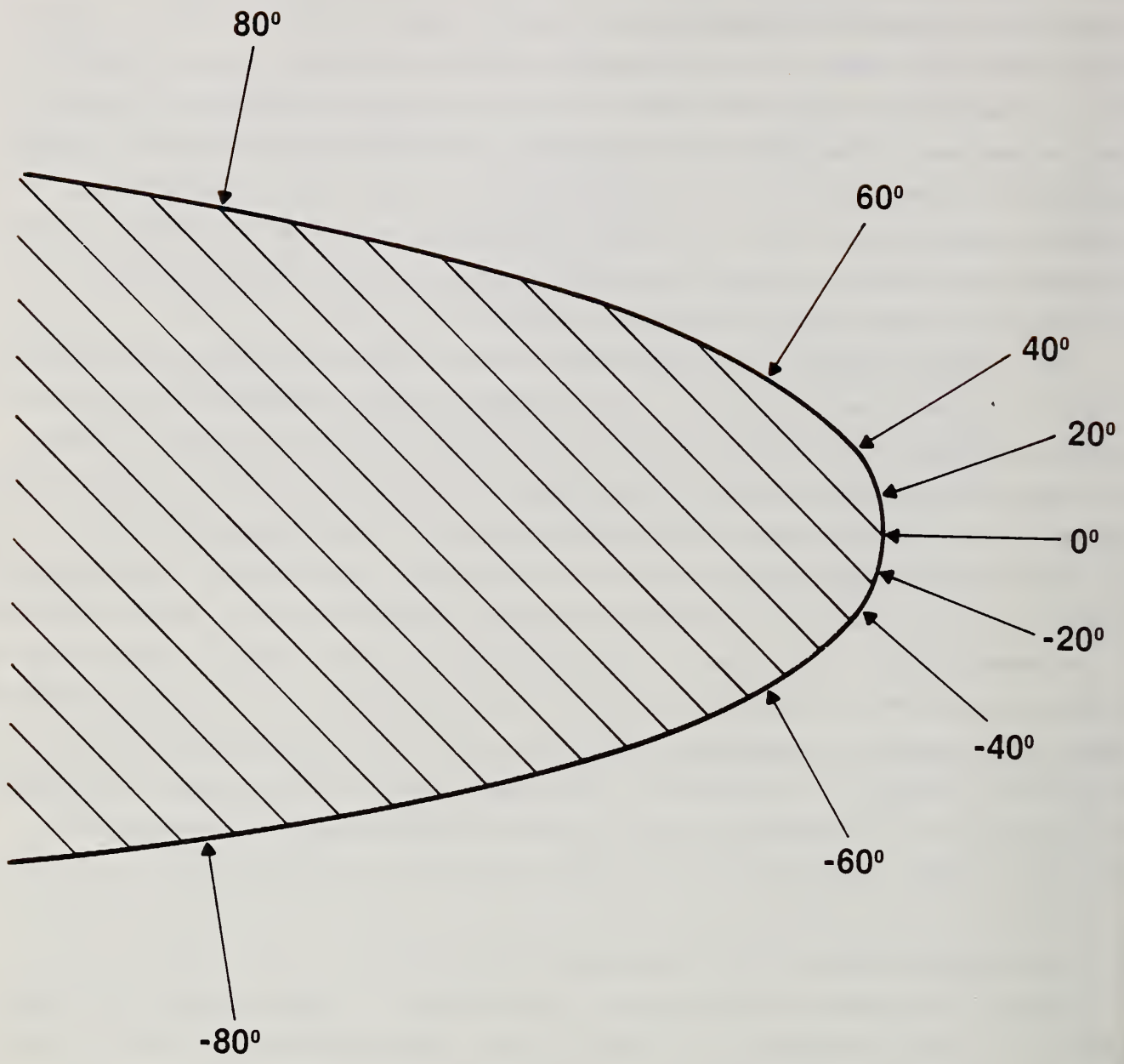


Figure 5 Figure showing the angular positions around the leading edge of the wing.

TABLE I

Descriptions of the individual flat specimens and the positions on the wing that were measured for roughness using both a stylus instrument and the optical MSG. The wing was manufactured from Nitronic 40 stainless steel.

<u>Specimen</u>	<u>Nominal Surface Finish</u> (μm)	<u>Type of</u> <u>Stainless Steel</u>
1	?	Nitronic 40 (N40)
3	0.2	N40
5	0.2	AF-1410
6	0.4	AF-1410
7	0.2	13-8
8	0.4	13-8
10	0.4	347
12	0.2	N40
13	0.4	N40
14	0.1	N40
15	0.2	347

<u>Wing Position</u>	<u>Description</u>
1, 2, 3	Topside.
4(-80°), 4(-60°), 4(-40°) 4(-20°), 4(0), 4(20°) 4(40°), 4(60°), 4(80°)	Around the leading edge of the wide end of the wing.
6(-80°), 6(-60°), 6(-40°) 6(-20°), 6(0), 6(20°) 6(40°), 6(60°), 6(80°)	Around the leading edge of the narrow end (outer tip) of the wing.
7, 8, 9	Topside, approaching the leading edge.

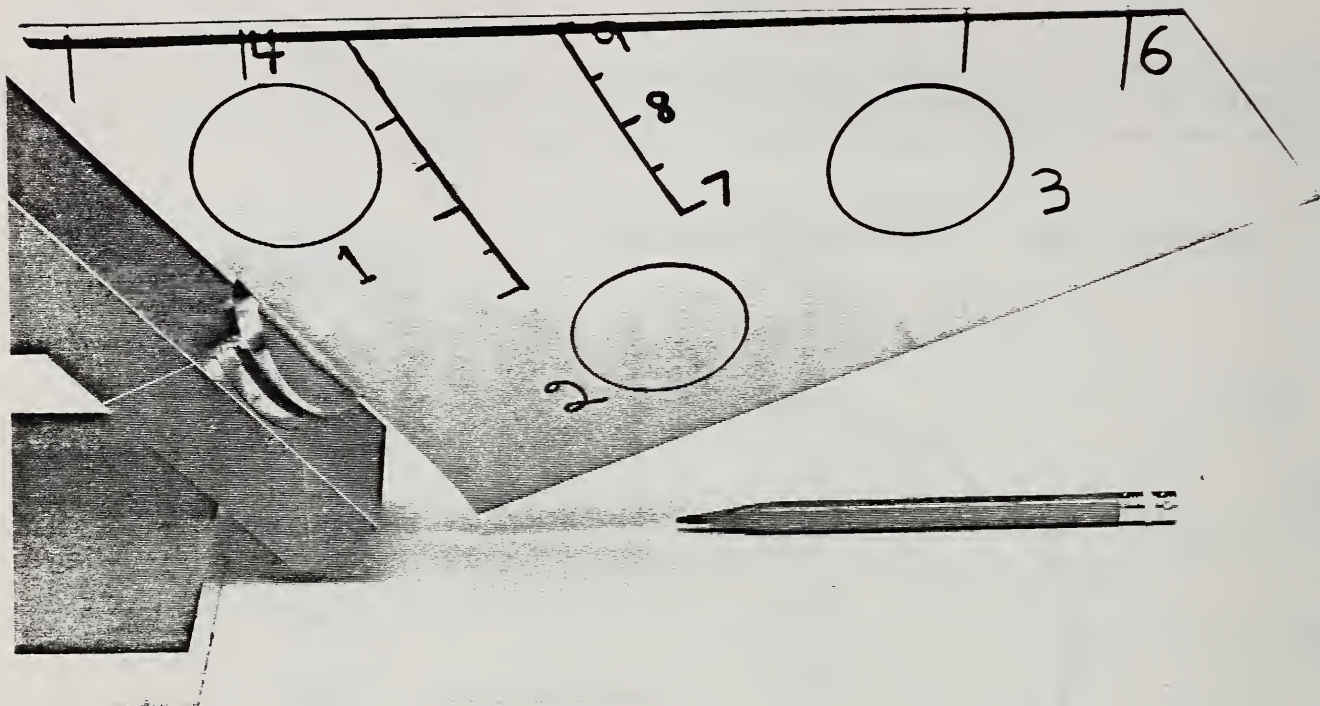


Figure 6 Photograph depicting the various positions on the wing (W-1 to W-9) that were measured. There was no W-5 position.

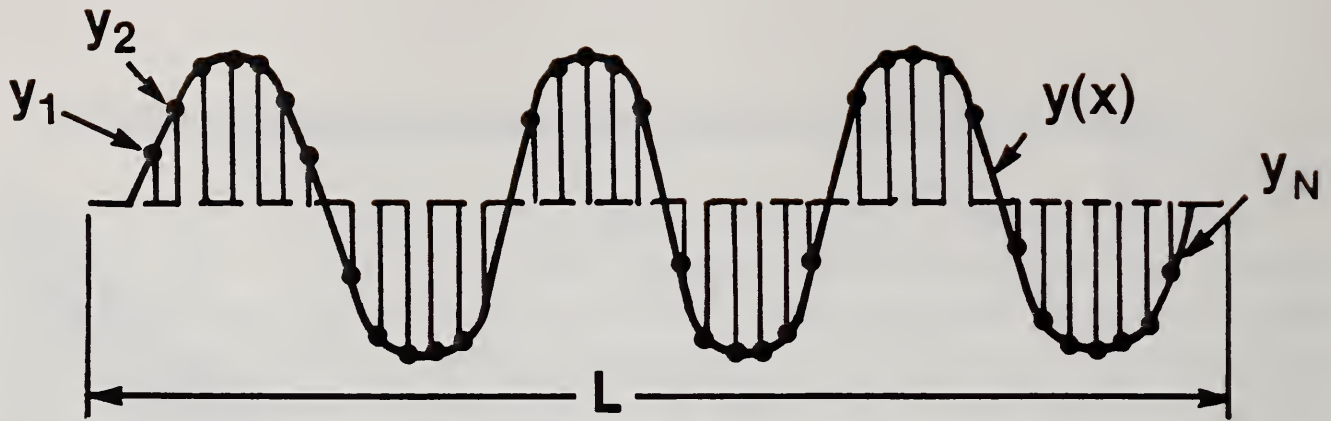
optically for S_N with the MSG and mechanically for rms roughness with a stylus instrument.

The stylus instrument is a Talysurf 6 model that contains an LVDT (linear variable differential transformer) transducer that gives a direct readout of the surface height under the stylus probe. As the stylus traverses the surface, its vertical motion is converted into a time varying electrical signal that accurately represents the surface peaks and valleys within the range and resolution limits of the instrument. The horizontal resolution is limited by the stylus tip width which was measured to be $\sim 5 \mu\text{m}$. The long wavelength sensitivity is determined in a standard way by the high pass electrical filtering of the instrument [11] and specified in terms of a long wavelength cutoff. The cutoff for our measurements was 0.25 mm and the total evaluation length was 1.25 mm or a distance of five cutoff lengths. The vertical resolution was limited by the rms vertical noise of the instrument, and this was measured to be $0.01 \mu\text{m}$ by traversing an extremely smooth glass surface whose actual roughness was smaller than the instrumental noise. The vertical range was about $600 \mu\text{m}$.

For the flat specimens and the flatter positions on the wing, stylus traces were taken perpendicular to the lay of machining marks. However, for the more curved positions on the wing, particularly including positions 4, 6, and 9, traces were taken parallel to the leading edge to avoid introducing surface curvature effects into the roughness measurements.

Each location was measured for roughness average R_a and rms roughness R_q , two quantities defined in many of the national and international standards [11]. As shown in Fig. 7, R_a is the average deviation of the roughness profile from the mean line and R_q is the root mean square deviation. Table II shows the results for these parameters. Each R_a and R_q value given there is an average derived from profiles measured at either 5 or 9 positions, as shown in column 2.

Two sets of S_N values are shown in Table III, representing values measured for two different MSG heads. One head, described before, produced a 1.8 mm illumination spot size and an angular detection range of $\pm 15^\circ$ about the central angle. The other had a 0.3 mm illumination spot size and an angular range of approximately $\pm 12^\circ$. The second gauge head was tested for comparison purposes because it was reckoned that the smaller spot size would render this gauge less sensitive to surface curvature. However, results taken with the 0.3 mm head are also expected to be more variable than that of the 1.8 mm head because the



- R_a = Average Deviation of Profile $y(x)$ from the mean Line

= Total Shaded Area / L

$$= \frac{1}{L} \int_0^L |y(x)| dx \cong \frac{1}{N} \sum |y_i|$$
- R_q = rms Deviation . . .

$$\cong \sqrt{\frac{1}{N} \sum y_i^2}$$

Figure 7 Schematic diagram showing the definitions of R_a and R_q as obtained from surface profiles.

TABLE II

Results for roughness average R_a and rms roughness R_q measured with a stylus instrument with 0.25 mm cutoff. Column 2 shows the number of different positions (5 or 9) used for the stylus measurements. The uncertainties represent statistical uncertainties of 1 standard deviation over the 5 or 9 positions.

<u>Specimen or Wing Position</u>	<u>Number of Stylus Positions</u>	R_a (μm)	R_q (μm)
Specimen: 1	9	0.221 \pm 0.016	0.284 \pm 0.020
3	9	0.121 \pm 0.006	0.156 \pm 0.008
5	9	0.083 \pm 0.006	0.112 \pm 0.012
6	9	0.29 \pm 0.03	0.38 \pm 0.04
7	9	0.106 \pm 0.005	0.138 \pm 0.008
8	9	0.214 \pm 0.011	0.280 \pm 0.016
10	9	0.273 \pm 0.019	0.355 \pm 0.025
12	9	0.172 \pm 0.009	0.220 \pm 0.013
13	9	0.188 \pm 0.014	0.244 \pm 0.019
14	9	0.044 \pm 0.002	0.055 \pm 0.003
15	9	0.130 \pm 0.009	0.166 \pm 0.012
Wing: 1	9	0.055 \pm 0.005	0.071 \pm 0.010
2	9	0.057 \pm 0.006	0.077 \pm 0.019
3	9	0.087 \pm 0.006	0.111 \pm 0.010
7	9	0.055 \pm 0.005	0.073 \pm 0.012
8	9	0.063 \pm 0.005	0.081 \pm 0.008
9	9	0.069 \pm 0.012	0.095 \pm 0.028
4 (80°)	5	0.056 \pm 0.002	0.072 \pm 0.003
4 (60°)	5	0.102 \pm 0.023	0.15 \pm 0.06
4 (40°)	5	0.167 \pm 0.017	0.223 \pm 0.024
4 (20°)	5	0.64 \pm 0.20	0.86 \pm 0.22
4 (0°)	5	0.47 \pm 0.09	0.65 \pm 0.10
4 (-20°)	5	0.36 \pm 0.04	0.49 \pm 0.08
4 (-40°)	5	0.21 \pm 0.03	0.26 \pm 0.04
4 (-60°)	5	0.109 \pm 0.014	0.141 \pm 0.021
4 (-80°)	5	0.071 \pm 0.007	0.091 \pm 0.010
6 (80°)	5	0.127 \pm 0.014	0.165 \pm 0.017
6 (60°)	5	0.224 \pm 0.021	0.290 \pm 0.027
6 (40°)	5	0.31 \pm 0.05	0.40 \pm 0.07
6 (20°)	5	0.37 \pm 0.04	0.47 \pm 0.07
6 (0°)	5	0.51 \pm 0.21	0.66 \pm 0.26
6 (-20°)	5	0.46 \pm 0.10	0.59 \pm 0.14
6 (-40°)	5	0.30 \pm 0.11	0.38 \pm 0.14
6 (-60°)	5	0.156 \pm 0.014	0.198 \pm 0.020
6 (-80°)	5	0.13 \pm 0.03	0.17 \pm 0.05

TABLE III

S_N values taken with two different probes having spot sizes of ~ 1.8 and ~ 0.3 mm. The uncertainties represent statistical uncertainties of one standard deviation. In some cases, no uncertainty is given, either because only one reading was taken or because two readings were taken and they were identical. The total number of observations and the number of different observers for each reading are also shown. Several of the readings were questionable (?) due to their proximity to the leading edge.

<u>Specimen</u> <u>or</u> <u>Wing Position</u>	<u>1.8 mm Probe</u>		<u>0.3 mm Probe</u>	
	S_N	#Readings, #Observers	S_N	#Readings, #Observers
Specimen: 1	86.0 \pm 2.2	4, 4	90.1 \pm 2.7	2, 2
3	77.9 \pm 1.5	4, 4	83.4 \pm 0.9	2, 2
5	45.3 \pm 1.0	4, 4	47.7 \pm 0.1	2, 2
6	88.5 \pm 2.2	4, 4	92.4 \pm 0.1	2, 2
7	73.0 \pm 1.4	4, 4	75.4 \pm 4.1	2, 2
8	84.6 \pm 2.0	4, 4	89.4 \pm 5.7	2, 2
10	87.8 \pm 1.3	4, 4	91.8 \pm 0.8	2, 2
12	83.5 \pm 3.0	3, 2	87.8 \pm 4.5	3, 1
13	87.0 \pm 1.7	4, 4	89.5 \pm 3.7	2, 2
14	39.3 \pm 2.0	4, 4	41.7 \pm 0.6	2, 2
15	72.1 \pm 1.4	4, 4	74.0 \pm 0.4	2, 2
Wing: 1	25.9 \pm 1.7	4, 4	27.3	2, 2
2	20.7 \pm 1.0	4, 4	25.2 \pm 2.4	2, 2
3	34.1 \pm 2.1	4, 4	33.5 \pm 2.3	2, 2
7	23.4 \pm 0.6	4, 2	26.2 \pm 0.5	3, 1
8	22.7 \pm 0.8	4, 2	23.0 \pm 0.9	3, 1
9	21.8 \pm 1.7	3, 1	23.1 \pm 0.6	3, 1
4(80°)	27.0 \pm 0.8	3, 2	27.1 \pm 1.6	2, 1
4(60°)	42.7 \pm 3.2	3, 2	37.8 \pm 3.3	4, 2
4(40°)	? 85.2	1, 1	64.4	1, 1
4(20°)	? 89.8	1, 1	? 62.2 \pm 0.9	2, 2
4(0°)	? 85.7	1, 1	? 71.0 \pm 4.5	2, 2
4(-20°)	? 89.3	1, 1	? 82.6 \pm 6.0	3, 1
4(-40°)	? 91.0	1, 1	72.7 \pm 1.5	3, 2
4(-60°)	48.2 \pm 1.7	3, 2	52.4	1, 1
4(-80°)	29.1 \pm 0.7	3, 1	33.2 \pm 1.9	2, 1
6(80°)	56.3 \pm 0.4	2, 2	56.6 \pm 2.6	2, 1
6(60°)	80.9 \pm 2.1	2, 2	? 86.8	1, 1
6(40°)	--	--	82.3 \pm 1.5	2, 1
6(20°)	--	--	? 75.6 \pm 6.9	2, 1
6(0°)	--	--	? 78.2	1, 1
6(-20°)	--	--	? 79.0	1, 1
6(-40°)	--	--	? 77.5 \pm 4.0	2, 1
6(-60°)	73.4 \pm 4.4	2, 2	? 83.5	1, 1
6(-80°)	51.3 \pm 6.4	2, 2	53.8 \pm 1.2	2, 1
Reference Mirror	5.1 \pm 0.1	2, 2	5.8 \pm 0.1	2, 2

smaller spot is probing a smaller statistical sample of the surface peaks and valleys. The total number of readings that went into each of the values and the number of different observers are also shown in adjacent columns to the values themselves.

A principal objective for testing the MSG was to show the correlation between the S_N results and the R_q results. Accordingly, the R_q values have been plotted versus the S_N values taken with the 1.8 mm head (termed $S_N(1.8)$) in Fig. 8, and a functional correlation has been developed between them.

Two observations constrained the form of the function that we fitted for R_q vs S_N . First, the curve has an asymptote at $S_N = 100$. An S_N value of 100 corresponds to a flat angular distribution having uniform scattering intensity at all angles. For a random surface finish, the angular distribution is a bell shaped curve having its maximum in the specular direction. The distribution generally becomes broader as the roughness increases, but it should approach a flat distribution only as the value of R_q becomes very large. Hence, the asymptote at $S_N = 100$.

Second, the spreading of the optical beam in the gauge is such that the value of S_N equals 5 when the rms roughness R_q is essentially equal to zero. This is the situation that occurs when the MSG is tested with smooth optical surfaces. Hence, the function $R_q(S_N)$ should pass through the point (5,0).

In view of these constraints, the following formula for R_q was chosen:

$$R_q (\mu\text{m}) = a(S_N - 5) + \frac{b(S_N - 5)}{95(100 - S_N)} \quad (3)$$

having the parameters a and b. These were fitted to the data by a linear least squares method. The resulting best fit values for a and b, rounded to three significant figures, were

$$\begin{aligned} a &= 0.00248 \pm 0.00063 \mu\text{m} , \\ b &= 1.43 \pm 1.03 \mu\text{m} , \end{aligned} \quad (4)$$

where the uncertainties in the fitted parameters represent estimates of one standard deviation for each parameter. The fitted curve is the lower one in Fig. 8.

Rq vs. SN(1.8) - NASA Surfaces

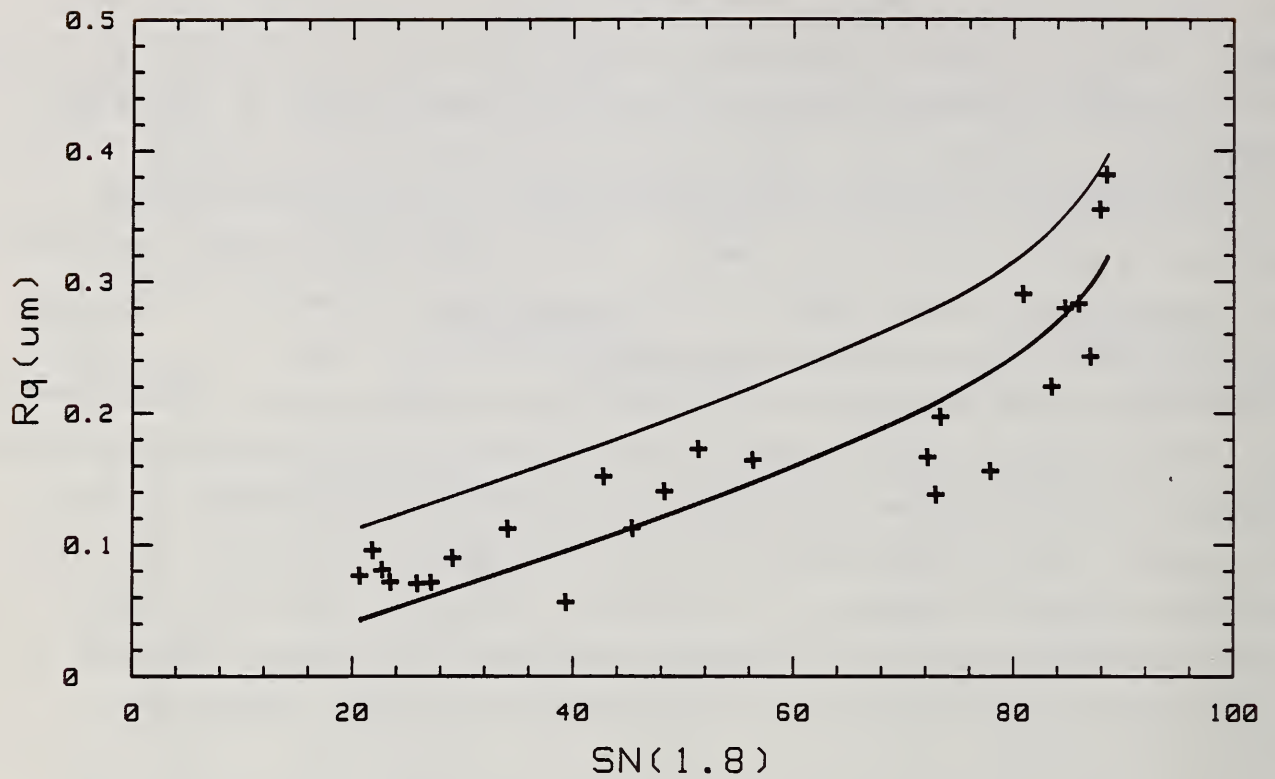


Figure 8 R_q values as measured with a stylus instrument vs. the S_N values obtained from the MSG with 1.8 mm spot size. The lower curve is the best fit to the data points represented by Eqs. 3 and 4. The upper curve is the 95 percent upper confidence limit.

For the results in Fig. 8, we calculated a coefficient of determination r^2 [12,13]. This statistic is similar to the correlation coefficient and is a standard approach for expressing how well the variation in the R_q data is accounted for by the fitted curve. For the nonlinear model of Eq. (3), the formula for r^2 is given by

$$r^2 = \frac{\sum_i \hat{R}_{qi} R_{qi} - n\bar{R}_q^2}{\sum_i R_{qi}^2 - n\bar{R}_q^2}, \quad (5)$$

where R_{qi} is the set of 25 R_q values, \bar{R}_q is the mean of these data and \hat{R}_{qi} is the set of R_q values predicted by the fitted curve. The calculated value for r^2 was 0.81 representing a fairly good correlation between the S_N vs. R_q data and the fitted curve, considering that the data include points taken on four different materials and with widely differing surface curvatures.

This empirical model of Eqs. 3 and 4 can be rewritten by combining terms to yield the following, more conventional form:

$$R_q(\text{mm}) = -0.0275 + 0.00248S_N + 1.43/(100-S_N), \quad (6)$$

which represents the same function as Eqs. 3 and 4. We particularly note that the three constants are not independent. The leading constant is related to the other two by the constraint that $R_q = 0$ when $S_N = 5$.

The adequacy of this model was further evaluated by comparing it with one having three arbitrary constants where the aforementioned constraint is relaxed. That is, where

$$R_q = a' + b'S_N + c'/(100-S_N). \quad (7)$$

Once again, a linear least squares technique was used to find the best values of a' , b' and c' yielding a result

$$R_q = 0.0346 + 5.52 \times 10^{-4} S_N + 2.92/(100-S_N). \quad (8)$$

We then tested the significance of adding the third parameter to the model by calculating the F-statistic [14], a method for comparing the two models (3),

(4), and (8). First, we calculated the sum of the squares of the deviations between the data points and the fitted curve for both mathematical models, and these quantities were divided by the number of degrees of freedom for each. Then the ratio (F) between these quantities was calculated.

$$F = \frac{22 \sum_{i=1}^{25} (R_{qi} - \hat{R}_{qi2})^2}{23 \sum_{i=1}^{25} (R_{qi} - \hat{R}_{qi3})^2} = 1.41, \quad (9)$$

where \hat{R}_{qi2} is the set of R_q values predicted by the two parameter model; \hat{R}_{qi3} is the set of R_q values predicted by the three parameter model, and 22 and 23 are the number of degrees of freedom for each model. The above value of 1.41 falls well within the ninety percent confidence limits of 0.49 and 2.04 for the F-statistic obtained from a modified version of the OMNITAB statistical software package [15]. This result implies that the simpler two parameter model is statistically reasonable and that there is little significance to adding the third parameter.

As a result of the foregoing analysis, we conclude that the S_N data from the MSG together with the reworked two parameter model given by Eq. 6 are appropriate for estimating the rms roughness of hand lapped stainless steel surfaces. We now discuss the S_N criteria that should correspond to the surface roughness acceptability criterion that R_q be less than $0.2 \mu\text{m}$ ($8 \mu\text{in}$). Given a particular measurement of S_N at some position, how confident can we be that the R_q value there is less than $0.2 \mu\text{m}$?

To provide an answer to this question, we require not only the best estimate of R_q as a function of S_N obtained with Eq. 6, but also the uncertainty estimate, $\pm \Delta R_q$. This quantity varies slightly over the range of the data but is approximately $\pm 0.075 \mu\text{m}$ and represents a 90% confidence interval. For an S_N value of 50.4, the expected value for R_q is $0.126 \mu\text{m}$ from Eq. (6), the estimated ΔR is $0.074 \mu\text{m}$, and the 90% confidence range is from $0.052 \mu\text{m}$ to $0.200 \mu\text{m}$. Since we would expect 5% of the R_q values to fall below this range and 5% above, that implies that for a measured S_N value of 50.4, the corresponding value of R_q would be expected to be smaller than $0.200 \mu\text{m}$ 95% of the time. Hence, the criterion of 50 for an acceptable surface discussed in Sec. 2. The criterion of 72 for a marginal surface is the value of S_N that corresponds to a best estimate

for R_q of 0.20 μm obtained from Eq. 6. Figure 8 shows the two curves from which the criteria were calculated.

The above arguments are derived from statistical considerations only and do not take into account potential systematic errors that might be caused by (1) systematic variations in the stylus measurements of roughness themselves, (2) a breakdown of the chosen model for certain types of surfaces, or (3) invalid S_N readings. These eventualities could cause errors that add to the estimated confidence intervals. Indeed, these eventualities could affect not only the correlation between stylus measurements and the MSG results but also the correlation between roughness measurements taken with different stylus instruments. For example, roughness values measured by a direct profiling instrument, such as ours, could differ from those measured with shop-type instruments, and these differences could vary depending on the surface curvature, the levelling conditions, and the instrument cutoff. However, the above potential sources of error are not expected to be problematical for our experiments or for subsequent use. We discuss these three sources individually.

Systematic errors in the roughness measurements could be caused first by error in the calibration of the vertical scale of the instrument. This possibility was investigated by measuring sinusoidal roughness standards with well known R_a values of 0.3, 1.0 and 3.0 μm . The errors between the measured and accepted R_a values for these standards were 2.1%, 0.9% and 0.5%, respectively. Therefore, this source of error is not expected to be significant.

A more important source of variation is the arbitrariness of measurement conditions for stylus instruments. Roughness is not an intrinsic property of a surface, and the results of measurements of rms roughness depend on the conditions under which the measurements were taken, the most important of these being the stylus width that usually limits the high frequency, short wavelength response of the instrument and the electronic cut off that limits the long wavelength response. Furthermore, measurements of rms roughness are much more sensitive to the long wavelength cut off than the short wavelength limit, because in general longer wavelengths have larger amplitudes [16].

In our measurements we used a stylus with a tip width of $\sim 5 \mu\text{m}$. Therefore the horizontal resolution of the measurements was approximately 5 μm . The long wavelength cutoff for our measurements was 0.25 mm, a value listed among the set of preferred values in the ANSI/ASME Standard B46.1-1985 [11] but shorter than

the most commonly used, standard value of 0.8 mm. The shorter cutoff was chosen for two reasons. First, surface curvature is a significant factor in some of the positions on the wing that we measured. The surface curvature, when superimposed on the profile of the roughness structure to be measured, can significantly increase the measured values of rms roughness. Therefore, a cutoff value of 0.25 mm masks the curvature effects and emphasizes the finer roughness structures better than one of 0.8 mm. Second, although the upper wavelength limit on the MSG changes with roughness height and is difficult to characterize, it tends to be quite short. That is, the optical gauge is sensitive to surface roughness wavelengths on the order of 100 μm or less rather than those near 1 mm. Therefore, the 0.25 mm cutoff of the stylus instrument is better matched to the spatial bandwidth of the MSG than the more standard 0.8 mm cutoff.

An example of the variability of roughness measurements with experimental conditions is shown in Fig. 9, where the R_q results as measured by two procedures are compared. Along the vertical axis are plotted the R_q results of measurements on nine NASA specimens using a Talystep instrument with a 0.1 μm stylus width, a 2 mm trace length, and an electrical signal that did not undergo high pass filtering. The bandwidth of measured wavelengths extends to approximately the 2 mm trace length, and this value might be taken as roughly the effective cutoff length of the profiles. Along the horizontal axis are plotted the R_q results for the same surfaces using the Talysurf 6 instrument with the 5 μm stylus tip, 1.25 mm trace, and 0.25 μm cutoff. The results taken with the longer cutoff are about 20% larger than those taken with the shorter cutoff, but the correlation between the two sets of data is very high. The coefficient of determination for a straight line fit through the data of Fig. 9 is 0.996.

We would prefer to correlate the optical data with roughness parameters that are closely linked to the functional characteristic of aerodynamic drag, but, as discussed in the introduction, much work remains to be done before proper roughness characterizations for aerodynamic drag will be known. Instead, we estimated a maximum specification for rms roughness of 0.2 μm for models in the NTF under extreme flow conditions [3] based on the concept of the admissible roughness for an aerodynamically smooth surface [9, 17] and on assumptions about the relationship between admissible roughness and rms [3]. Likewise, our selection of a 0.25 mm electrical cutoff for use in roughness measurements

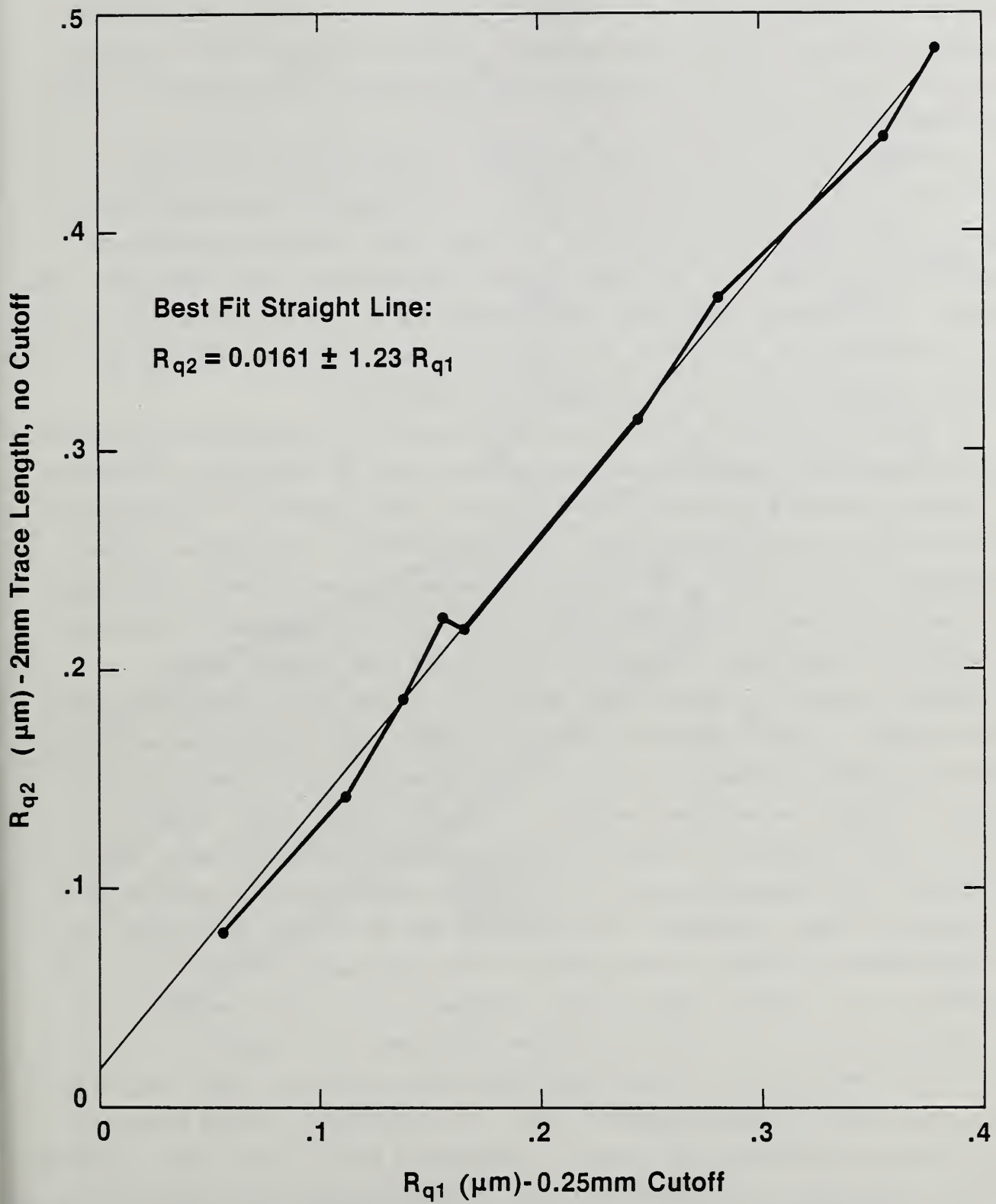


Figure 9 R_q values as measured with a Talystep plotted vs R_q values as measured with a Talysurf 6.

results from an estimation of the appropriate upper limit of the width of the roughness features found on these surfaces. Figure 9 implies that a scaling factor will result if the S_N values are compared with R_q values measured with a cutoff different from 0.25 mm.

In summary then, we have surmised that a roughness spatial bandwidth ranging from 5 μm to about 250 μm is useful for determining aerodynamic drag effects on hand lapped stainless steel surfaces, and we have correlated the response S_N of the MSG with the rms roughness measured over that bandwidth. The estimation of a maximum admissible rms roughness of 0.2 μm when measured with a 250 μm cutoff depends on a number of assumptions and should be verified by experiment in wind tunnels under extreme flow conditions.

The second potential source of systematic error is a breakdown of the model represented by Eq. 3. We have tried to minimize this by including in the study only similar stainless steel surfaces finished by hand lapping. The comparator approach should be valid when a small class of specimens with similar surface topographies is the subject for correlation between two measurement techniques. Other classes of specimens would produce quite different responses in the MSG even though such specimens had similar R_q 's to the ones studied here.

Finally, invalid S_N readings can result if the MSG is not properly aligned on the surface or if the surface curvature is high. Misalignment causes the scattering pattern to miss the diode array as shown in Fig. 3, resulting in a low total intensity value I and perhaps an unstable value of S_N . Surface curvature along the same direction as the long axis of the diode array leads to an increase in the apparent value of S_N over that which would be measured on a flat surface of equal roughness. Both problems may be avoided by staying away from the asymmetric, highly curved sections near the leading edges of the wing. Unfortunately, the leading edges are the critical places, where roughness can most affect drag, and hence where roughness measurement is important.

We have made empirical studies concerning the question of how close to the leading edge valid S_N readings may be taken. We did this by taking polar maps of S_N at several positions very close to the leading edge of the wing. As shown in Fig. 10, the MSG was held vertically in its stand and set down upon the wing so that the V-groove of the nosepiece cradled the curved surface. The wing itself was mounted in a gimbel so that it could be rotated about its leading edge. That way the angle θ of the gauge with respect to the leading edge could be varied and measured. Then S_N and I were measured as a function of the

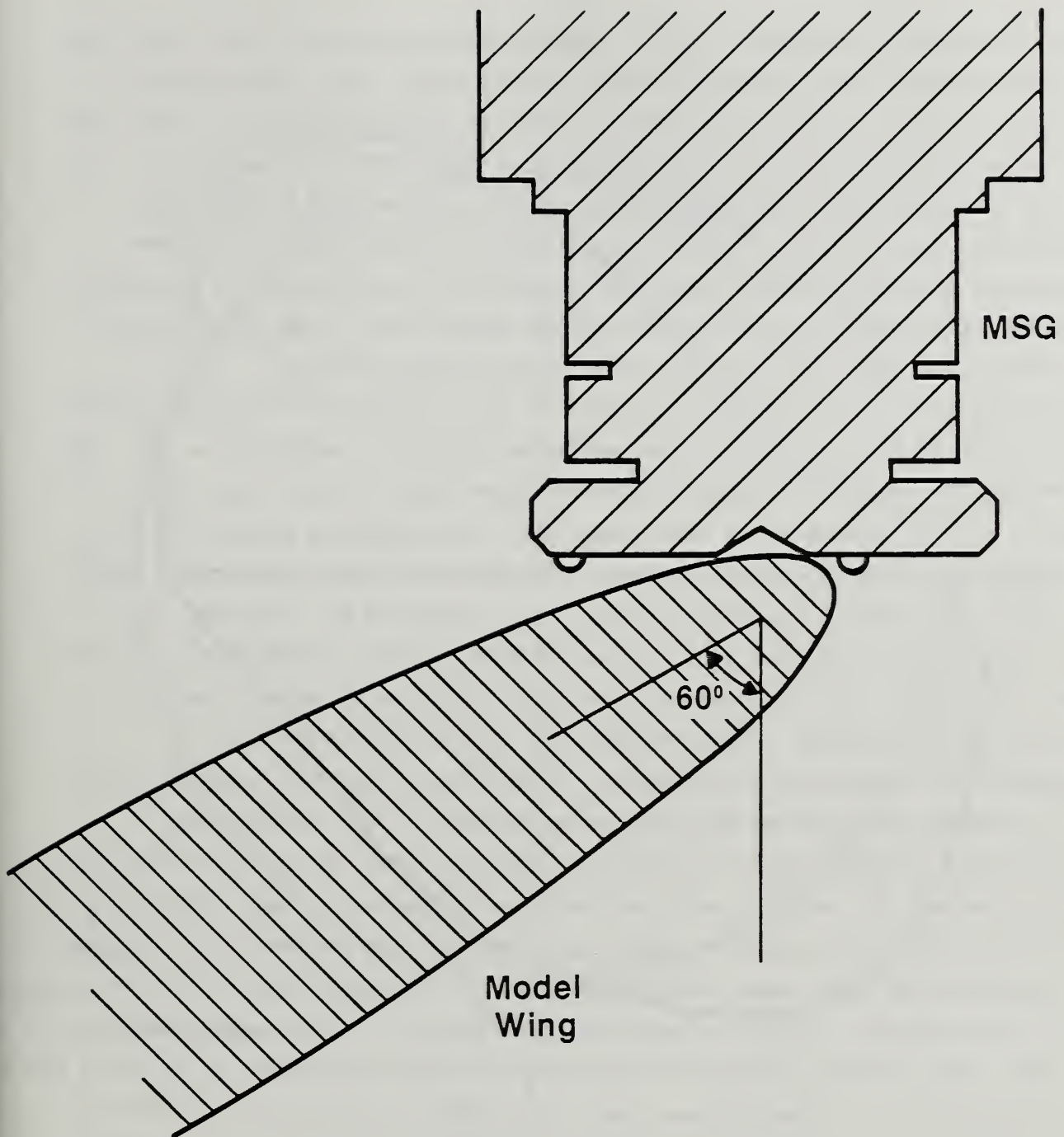
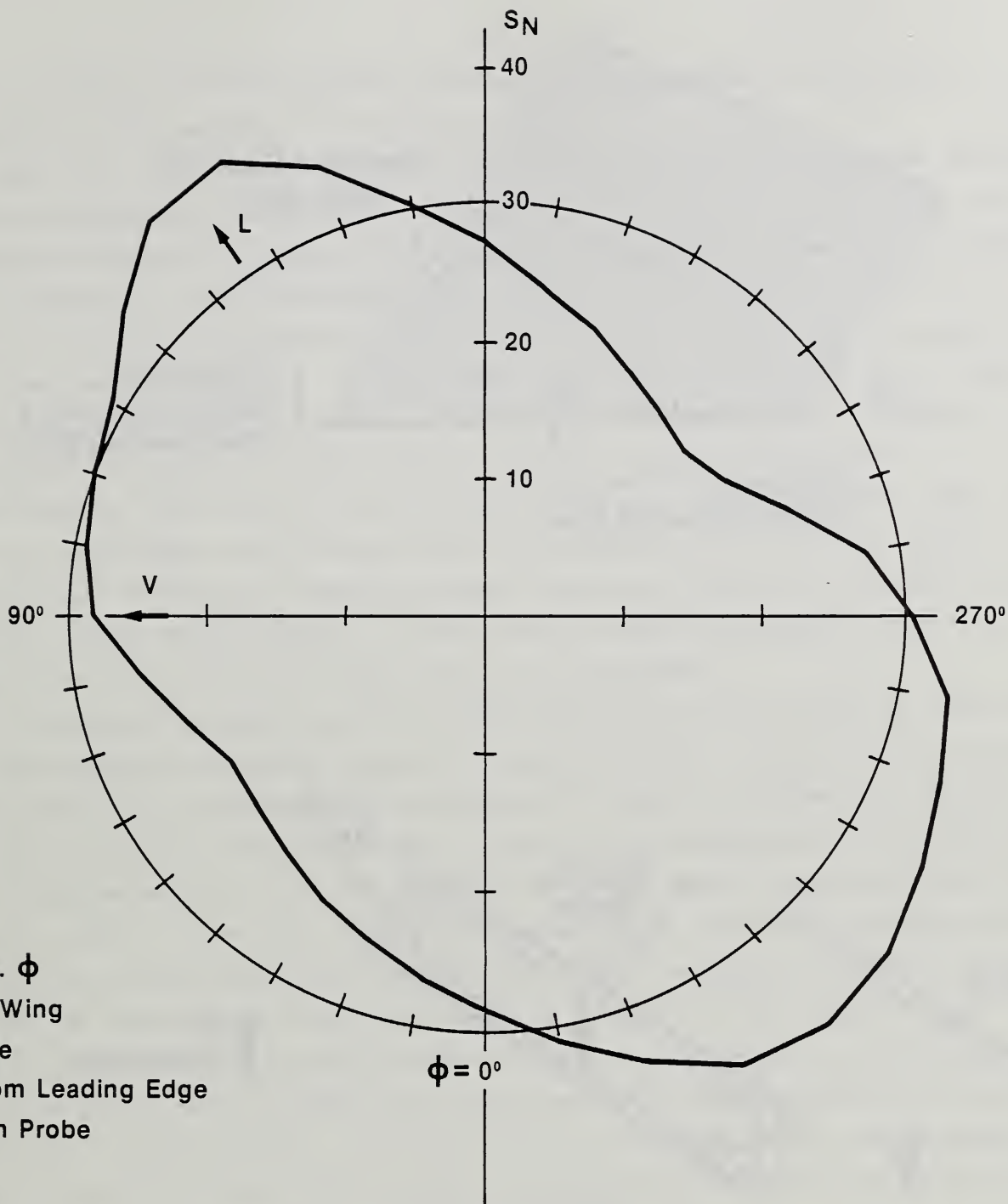


Figure 10 Schematic diagram showing alignment of the MSG for a reading at an angle θ of about 60° topside near the leading edge of the wing.

azimuthal angle ϕ . Altogether S_N vs ϕ was measured in areas 4 and 6 (see Fig. 6) at nine angular positions each at the leading edge: with the wing held vertically ($\theta = 0^\circ$), at four positions on the top side ($\theta = 20^\circ, 40^\circ, 60^\circ$ and 80°), and at four positions on the bottom ($\theta = -20^\circ, -40^\circ, -60^\circ$ and 80°). The $+80^\circ$ and -80° positions were located near the top and bottom of the wing, respectively (see Fig. 5). The 0.3 mm probe was initially used for these measurements because its small spot was thought to be preferable to the other. Subsequent measurement near the leading edge showed the 1.8 mm probe to give more stable readings, so polar maps were then gathered with it.

The map for the 60° location in the W-4 area around the front edge of the wing is shown in Fig. 11. Its shape may be explained by referring to Fig. 12a, a schematic picture of the topside near the front edge of the wing itself. The direction of the lapping marks that constitute the roughness pattern of the surface and the direction of the highest curvature are shown along with the approximate position of the measured area at an angle of 60° topside. The scattering pattern from this part of the surface is shown schematically in the center of Fig. 12b. It is broadened from top to bottom by geometrical scattering from the curve of the surface and in the NE-SW direction by diffraction from the surface roughness. By contrast, the left hand pattern of Fig. 12b schematically shows the scattering pattern if the surface has unidirectional roughness but no curvature, and the right hand side of Fig. 12b shows the pattern for surface curvature with no roughness. These infrared patterns have been inferred from observations of visible patterns obtained by scattering a He-Ne laser beam from the surface. The orientation of the diode array in the detector for an optimum roughness reading is depicted as well in Fig. 12b. This orientation has the diode array aligned parallel to the scattering pattern. It can be seen that the length of the pattern, and hence the S_N reading, at this orientation is only slightly increased by the surface curvature, since the direction of maximum curvature and the direction of maximum roughness are approximately 34° apart.

Figure 11 shows the polar map produced when the gauge is rotated. The direction of optimum alignment is indicated by the arrow L in Fig. 11 and the corresponding orientation of the diode array in Fig. 12b. Since the geometry is fairly symmetric, the polar map has maxima in the -40° and $+150^\circ$ directions clearly indicating the lay of the surface. The total intensity (I) is likewise



SN vs. ϕ
 NASA Wing
 Topside
 60° From Leading Edge
 1.8 mm Probe

Figure 11 Diagram of S_N vs. the azimuthal angle ϕ measured in area 4 at an angle θ of 60° topside with respect to the leading edge. The 1.8 mm probe was used. Vector L shows the direction of the lapping marks. Vector V shows the direction of the leading edge.

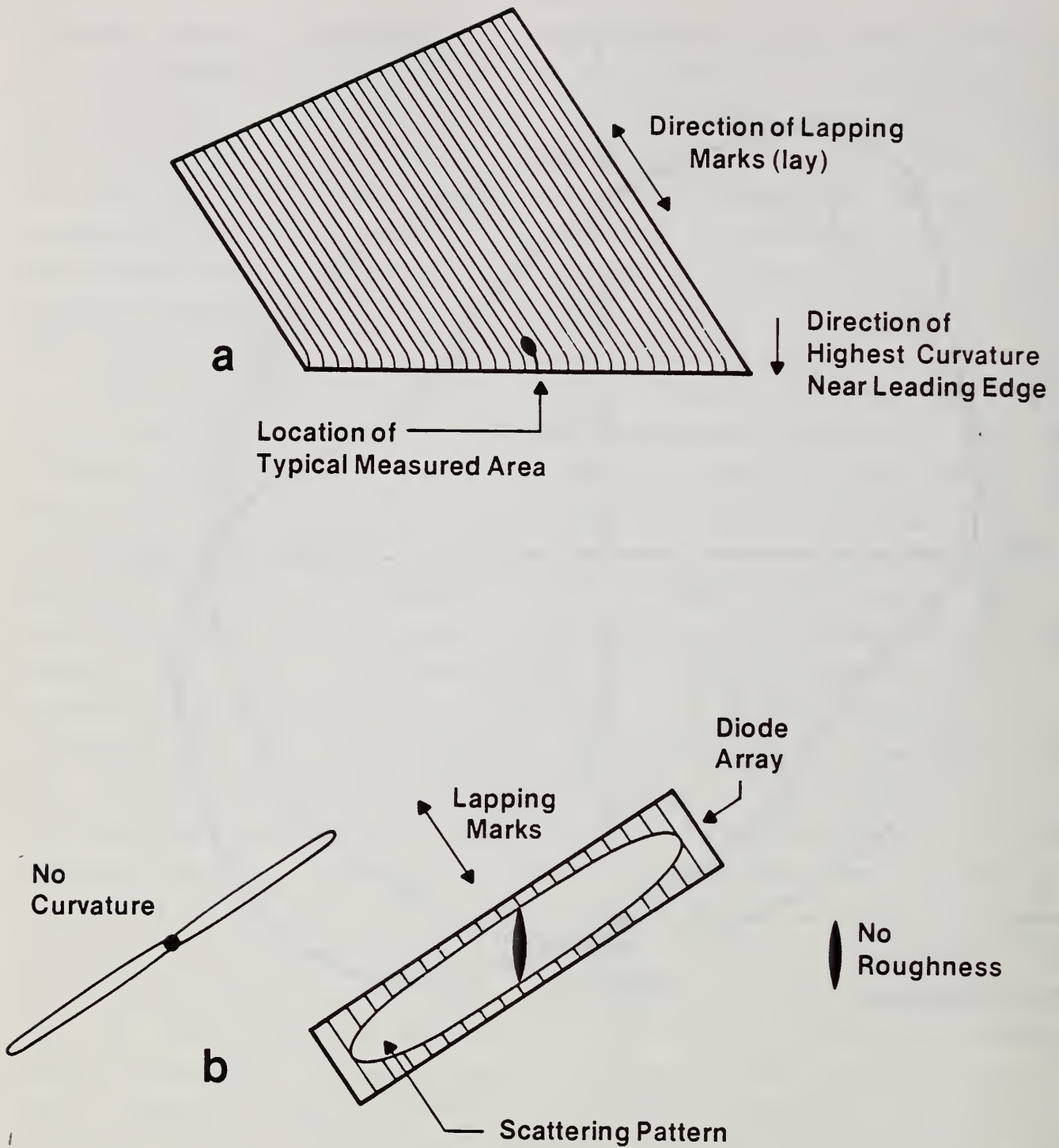


Figure 12 (a) Schematic diagram of the leading edge of a model wing showing the direction of the lapping marks and the direction of highest curvature around the location of a measured area.
 (b) Heuristic diagram of the optical scattering pattern overlaying the diode array detector rotated for a maximum S_N reading such as the one at $\phi = 150^\circ$ in Fig. 11. The two satellite patterns correspond to cases involving no curvature or no roughness.

fairly strong in the two optimum directions indicating good translational alignment of the pattern on the diode array.

When the illuminated area gets too close to the leading edge, the surface curvature becomes so large that the symmetry of the S_N vs. ϕ curve about the roughness direction is lost and the intensity decreases because of misalignment. Valid readings of the scattering pattern are no longer possible. Figure 13 shows the S_N pattern taken on the bottom of the wing in area 4 at an angle of 20° from the leading edge. The maximum value of S_N in the polar curve occurs along the direction of maximum curvature instead of the apparent roughness direction. In addition, total intensity at all angles is decreased significantly from that of the 60° topside position. From these and other data, we have established the criterion that the roughness direction must clearly be identifiable from the S_N reading and that the total intensity (I) must be larger than 50. With these criteria, we were able to take valid data to within an angle of 60° of the leading edge with the 1.8 mm probe.

In addition to the foregoing studies concerning the accuracy of the gauge, we also performed roughness studies of the wing itself. On Fig. 14 are plotted the values of R_q , measured with the Talysurf 6 stylus instrument, as a function of position on the wing. Positions 1-3 and 7-9 were taken on the top surface of the wing whereas positions -80° to $+80^\circ$ were taken around the leading edge at areas 4 and 6. It is clear from these measurements that the roughness degrades rapidly as one approaches the leading edge. This phenomenon is understandable in view of the fact that the model plane is finished by hand lapping. The gently curved top and bottom surfaces of the wing are easier to work by hand than the highly curved leading edge and hence have evidently received a more complete finishing process. Therefore for both areas 4 and 6, the roughness within about 60° of the leading edge is unacceptable because R_q is greater than $0.2 \mu\text{m}$.

This trend for the R_q value to increase around the edge is duplicated by the S_N data of Fig. 15. Once again the S_N values increase rapidly as the leading edge is approached. The points from area 4 labeled with "?" were of uncertain validity in view of the criteria previously discussed. The missing points from area 6, were either highly questionable or unmeasurable, taken, as they were, around the leading edge at the narrow end of the wing. Nevertheless, the optical data of Fig. 15 reveal the same trend in roughness near the leading edge as the stylus data of Fig. 14.

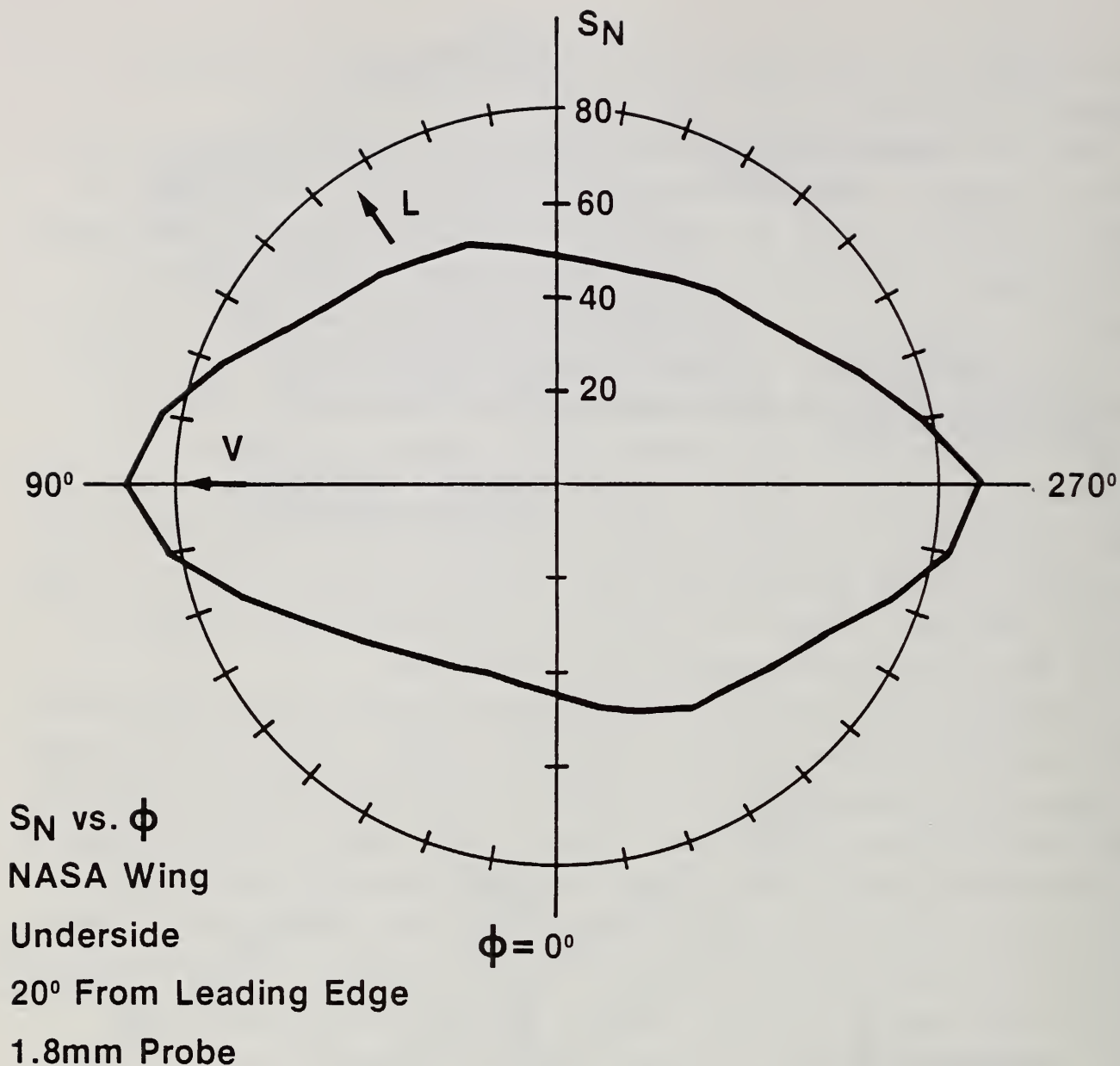


Figure 13 Polar graph of S_N vs. ϕ at a position of 20° underside from the leading edge, too close for a valid S_N reading. The 1.8 mm probe was used. The maximum S_N value now occurs when the diode array is aligned to detect the scattering pattern broadened by the edge curvature.

NASA Wing, RMS Roughness Measurements

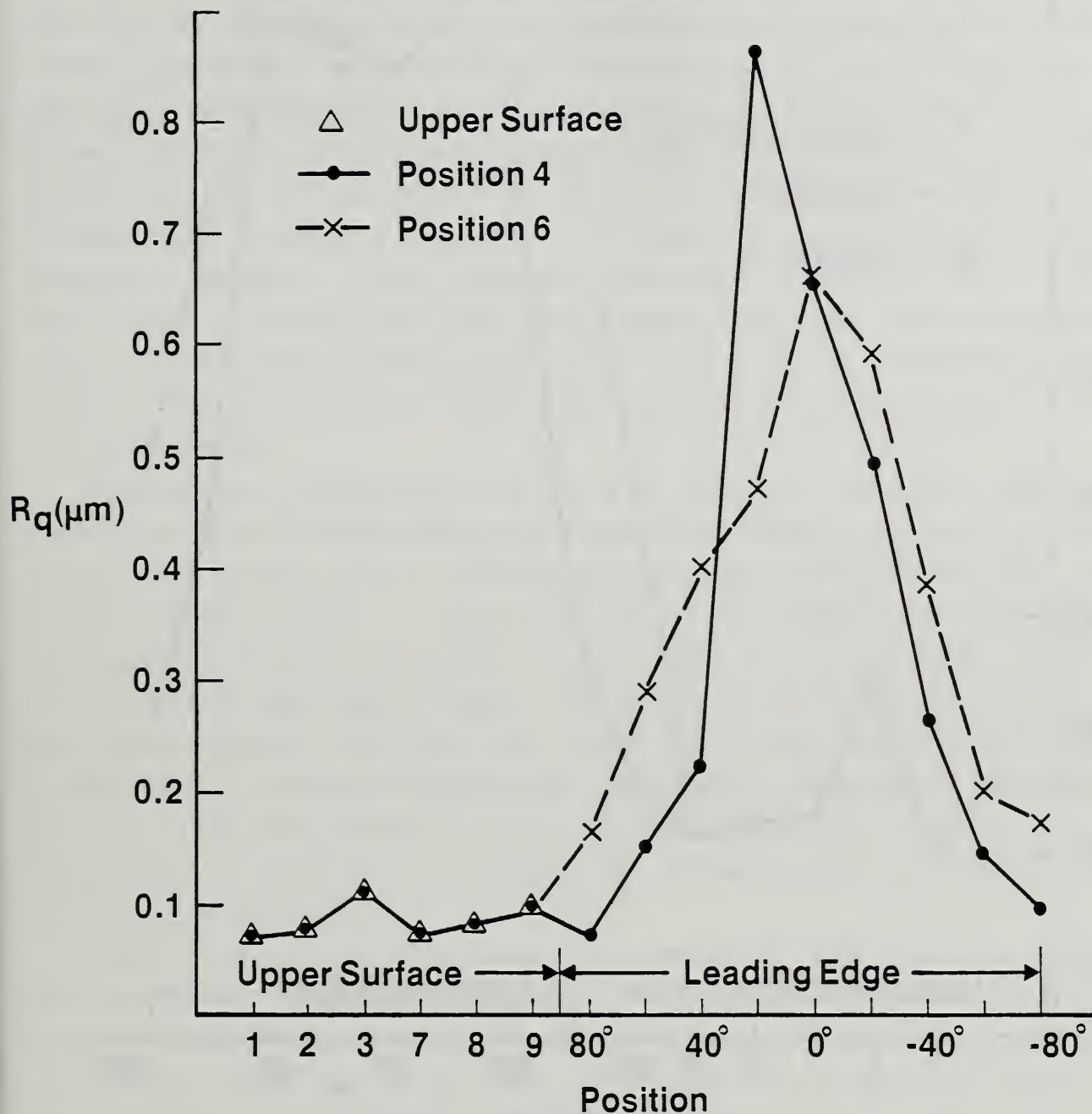


Figure 14 R_q measurements vs. position on the wing. The positions are shown in Figs. 5 and 6.

NASA Wing S_N Measurements with 1.8 mm Probe

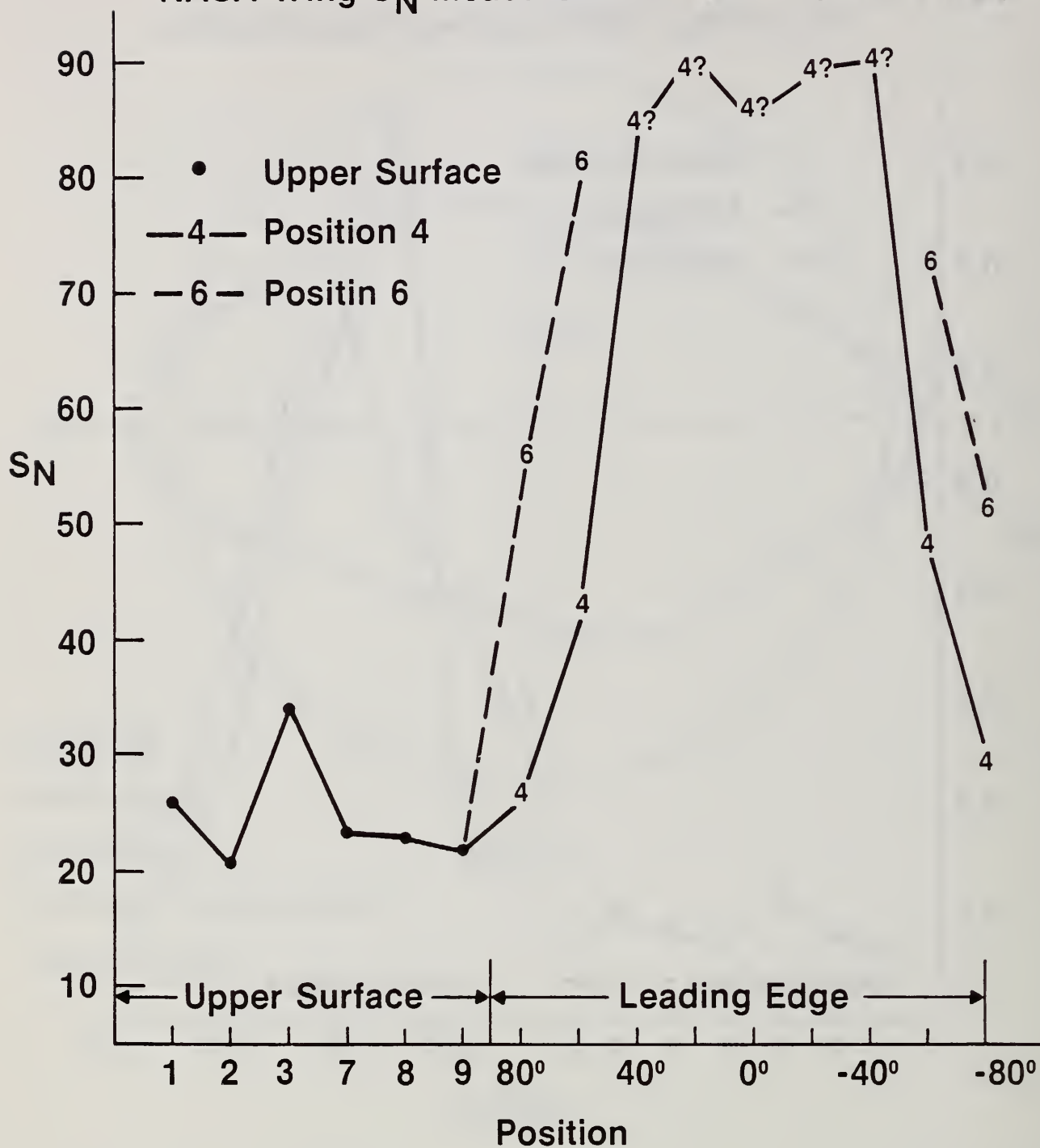


Figure 15 S_N obtained with the 1.8 mm probe vs. position on the wing. The values shown with question marks have uncertain validity due to proximity to the leading edge. Some values around area 6 were not measured at all due to misalignment difficulties near the leading edge.

The optical data for the two probe sizes are compared in Fig. 16. The probe with the 0.3 mm spot size has an advantage and a disadvantage with respect to the 1.8 mm probe. On the one hand, the probe with the smaller spot size should be less susceptible to having geometrical scattering from the curved surface affect the roughness scattering results. On the other hand, the smaller illumination spot averages over a smaller number of surface peaks and valleys. So the readings from the 0.3 mm probe should have more variability than those from the 1.8 mm probe. The 0.3 mm probe also seemed to suffer larger fluctuations in intensity near the leading edge of the wing, and we therefore reckoned it to be more susceptible than the 1.8 mm probe to misalignment of the surface around the y-direction (Fig. 3) due to the asymmetric curvature of the wing airfoil shape.

The correlation between the two set of S_N readings is excellent for those samples and those positions where both readings are expected to be valid, based on the signal intensity and S_N directionality criteria discussed earlier. This is shown clearly in Fig. 16. The coefficient of determination for these data with respect to a best fit straight line is 0.995. The points shown as question marks are those taken where either or both of the probe readings are of questionable validity according to the intensity and directionality criteria. Although, the 0.3 mm probe seemed to be susceptible to misalignment it appears that the 0.3 mm probe was able to take valid readings to within 40° of the leading edge in wing area 4 according to the intensity and directionality criterion (see Table III).

Figure 17 shows what happens when the S_N readings taken with the 0.3 mm probe are plotted versus the R_q readings. The correlation between S_N and R_q is similar to that of Fig. 8 except for the circled points. These were taken only 40° from the leading edge of the wing, and it appears that the S_N readings for these are biased lower than they should, given the R_q values. The source of this difficulty is not yet apparent. Our preliminary estimation is that the 0.3 mm probe is more sensitive to misalignment than the 1.8 mm probe and because of this, the probe does not accurately sample the angular distribution for points too close to the leading edges where the surface curvature is changing rapidly and where some misalignment around the y-axis of Fig. 3 is no doubt occurring.

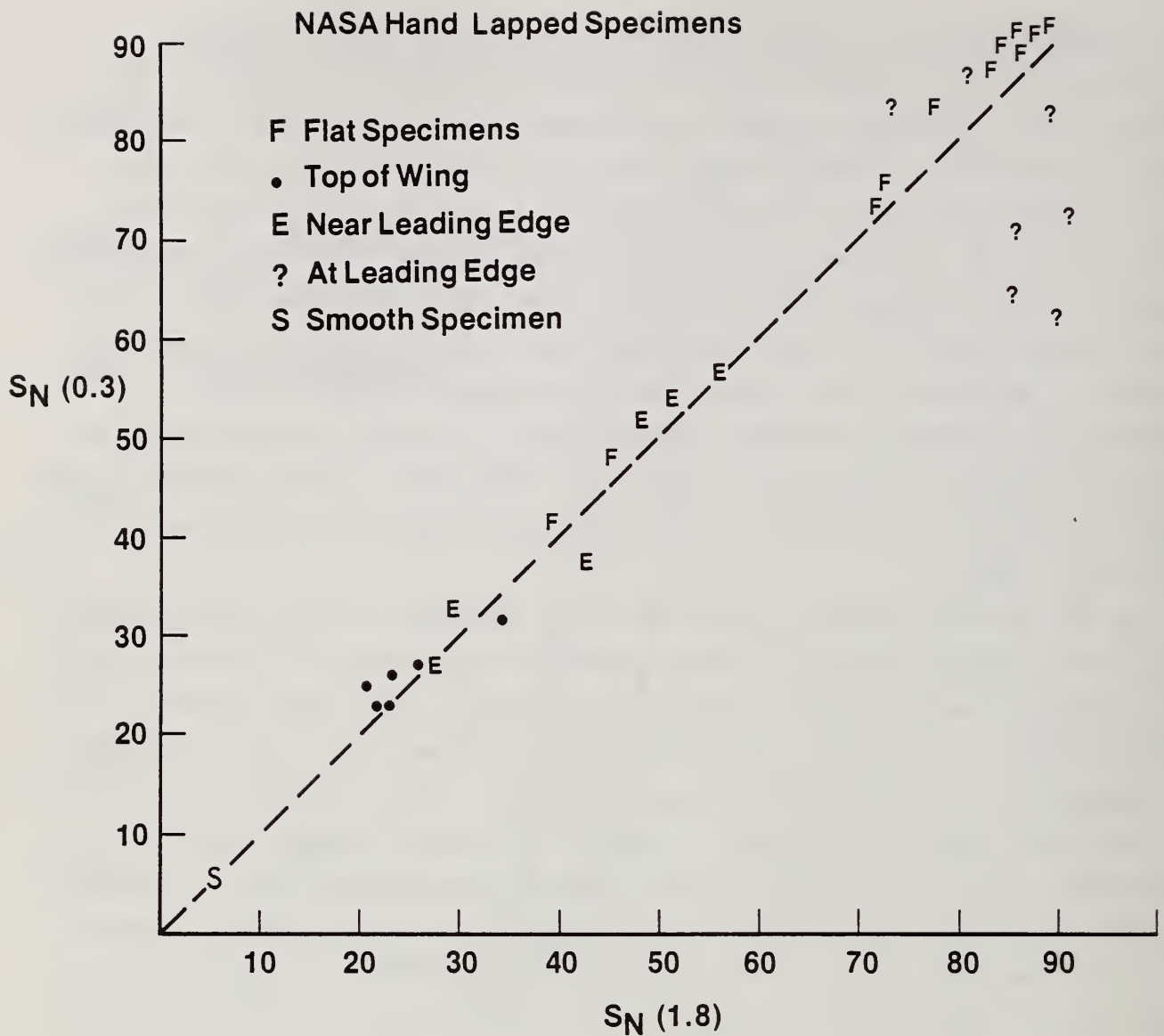


Figure 16 $S_N(0.3)$ vs. $S_N(1.8)$ for the flat specimens (F) and at various positions on the wing (coded). Point S was measured for the smooth reference specimen supplied by the manufacturer. The question marks are points of uncertain validity near the leading edge. The dashed line has a 45° slope and passes through the origin and is shown for reference.

Rq VS. SN(0.3) - NASA Surfaces

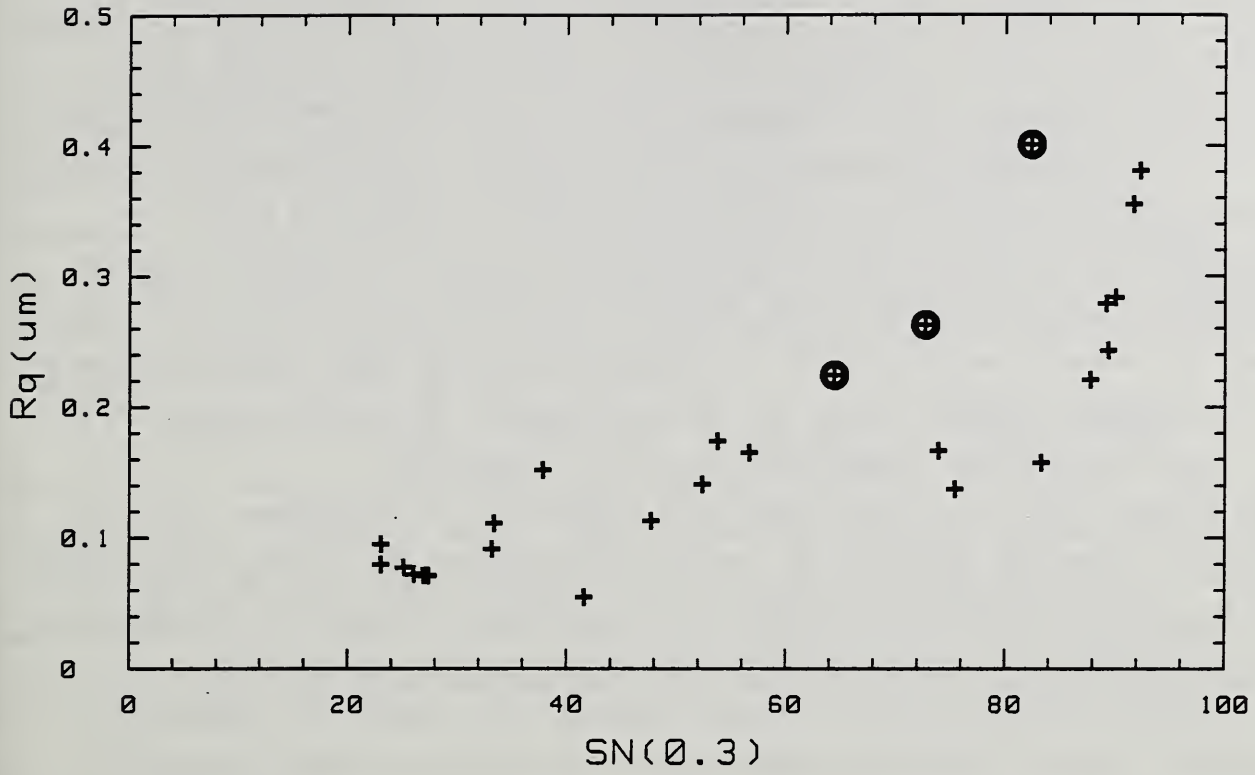


Figure 17 R_q measurements vs. S_N obtained with the 0.3 mm probe.

4. Limitations of the Present Instrument

The present instrument is useful as a working prototype to be tested for inspecting the roughness of wind tunnel model surfaces. Several features should be added to turn it into a useful, ergonomic instrument for the model shop.

To make the device more convenient to handle, two modifications should be made. First, the nosepiece should be fitted with some sort of handle so that it can be held solidly on the surface while the probe is rotated to find the optimum readings. Second, the control buttons should be located on the probe itself rather than the controller or should be implemented with foot switches. That way, an operator would not have to remove his or her hand from the probe to record a roughness reading. With the present system, the optimum alignment can be lost when the operator's hand moves to take a recording.

The present device is being used as a comparator for roughness. That is, estimations of the rms roughness R_q are being made based on the high correlation between R_q readings measured by stylus and S_N readings measured by the gauge. It would be preferable to derive rms values directly from the optical measurements and with a suitable theory, without resorting to the comparator approach that relies on previous measurements of similar surfaces to provide a calibration. To perform such a task, a proper theory to describe the light scattering needs to be developed along with an appropriate mathematical inversion technique to back out the rms roughness from the optical scattering angular distribution. The light scattering theory and the inversion technique would be installed as software on a laboratory computer to control the MSG. In its present state of development, the MSG is controllable by a computer through an RS-232 interface, and we have installed such a system on the inspection station of the Automated Manufacturing Research Facility (AMRF) at NBS [18]. We have also shown that the optical angular scattering pattern may be described fairly accurately if the topography of the surface is known from profiling measurements [4]. What is now needed is the appropriate inversion procedure to extract the rms roughness from the optical scattering pattern itself.

Another limitation is the difficulty of taking valid S_N readings within 60° of the leading edge of the wing because of the high curvature in those locations. It should be possible to make measurements right at the leading edge itself ($\theta = 0^\circ$), because that is a position of symmetry and the hand lapping marks should be parallel to the surface curvature there. Consequently, the broadening of the scattering pattern due to roughness effects should be

unaffected by the curvature. This is not the case in practice. Inspection of the leading edge shows that the directionality of the lapping marks varies considerably due to the workmanship of the finishing process. In some places the lapping marks are perpendicular to the leading edge. In others the marks are slanted with respect to the edge but parallel to the lapping marks on the top of the wing indicating a simple continuation of those marks by the machinist. In those places, it is not possible to take valid S_N readings since the curvature effects in the scattering cannot be separated from the roughness effects. In still others, the marks at the leading edge are continuations of the lapping marks on the bottom of the wing.

We, therefore, propose a refinement to the hand finishing process. If the machinist can make sure that the hand lapping strokes at the leading edge are perpendicular to the edge rather than simple continuations of the strokes on the top or bottom of the wings, the extra care might enable valid optical roughness measurements to be made with the MSG at the leading edge itself and might also lead to a better finished leading edge with improved aerodynamic properties.

5. Related Work

We have performed a number of other activities under contract with the NASA Langley Research Center. These have been thoroughly documented in previous publications [1-8], but a brief summary of the optical scattering work is given here as well.

We constructed a research instrument [1,5] that measures the light scattering distributions from rough surfaces. Named DALLAS, detector array for laser light angular scattering, it has the capabilities for varying the angle of incidence of laser light on the specimen and for collecting nearly the entire hemisphere of scattered radiation. We have used this instrument to characterize the light scattered from the surfaces of NASA hand lapped, stainless steel specimens and to test theories of optical scattering from rough surfaces.

Our initial experiments involved the measurement of the same surfaces with both the stylus technique and the DALLAS instrument. The key question in this work was whether or not the optical theory was capable of generating a quantitatively accurate description of the angular distribution of scattered light using knowledge of the surface topography obtained from surface profiles. The surface profiles were measured with the stylus technique, then digitized, and stored on a computer disk. A straightforward, but appropriate scattering

theory, using a phase integral approach, was applied to the profile data to yield a theoretical angular scattering distribution that could be compared to the one measured by DALLAS [5]. The technique was first applied to a set of ground specimens. The surface profiling data were taken at a lateral resolution of about $1.5 \mu\text{m}$ and the agreement between the theoretical and experimental angular distributions was moderately good [5]. Subsequently, we have measured nine hand lapped NASA specimens and improved the lateral resolution of the surface profile. The agreement between theory and experiment is quite good. A complete article based on this research will be published subsequently, but one typical result is shown in Fig. 18. Our preliminary estimation is that the small degree of disagreement between theory and data is due to lateral resolution limits of the surface profiles, but we require more analysis to confirm this.

From this work we can say that if one knows the surface topography, represented by the surface profiles, one can quantitatively describe the optical angular scattering distribution for moderately rough surfaces of the types studied with R_q 's up to about $0.3 \mu\text{m}$. This is a strong indication that the optical phase screen theory that we used is valid in the range of roughnesses exemplified by the NASA specimens.

The next step is to invert the scattering data to obtain accurate values of geometrical surface parameters such as the roughness height or average roughness spacing. The first experiments along these lines were performed for a set of six sinusoidal surfaces with differing amplitudes and spatial wavelengths [7,8]. The experimental scattering distributions consisting of sharply peaked, diffraction patterns, obtained with DALLAS operating in a special high resolution mode, were compared with theoretical calculations that relied on two variable parameters, the amplitude of the surface sine wave (which could be directly related to its R_a value) and the wavelength D . The values of the parameters that yielded the best fits between the data and the theory are shown in the right hand columns of Table IV. The agreement between these and the parameters measured by stylus shown in the middle columns is excellent. The parenthesis around the $800 \mu\text{m}$ value indicates that this surface was a special case. The diffraction peaks in the angular distribution were so closely spaced that they could not be individually resolved by the detector. This produced an ambiguity and a tradeoff between the best adjusted values of amplitude and wavelength. However, when a wavelength value of $800 \mu\text{m}$ was assumed in the

NASA S.S. Spec. #3; Incidence Angle=-54

Data measured with DALLAS _____

Theoretical Angular Distribtion. . .

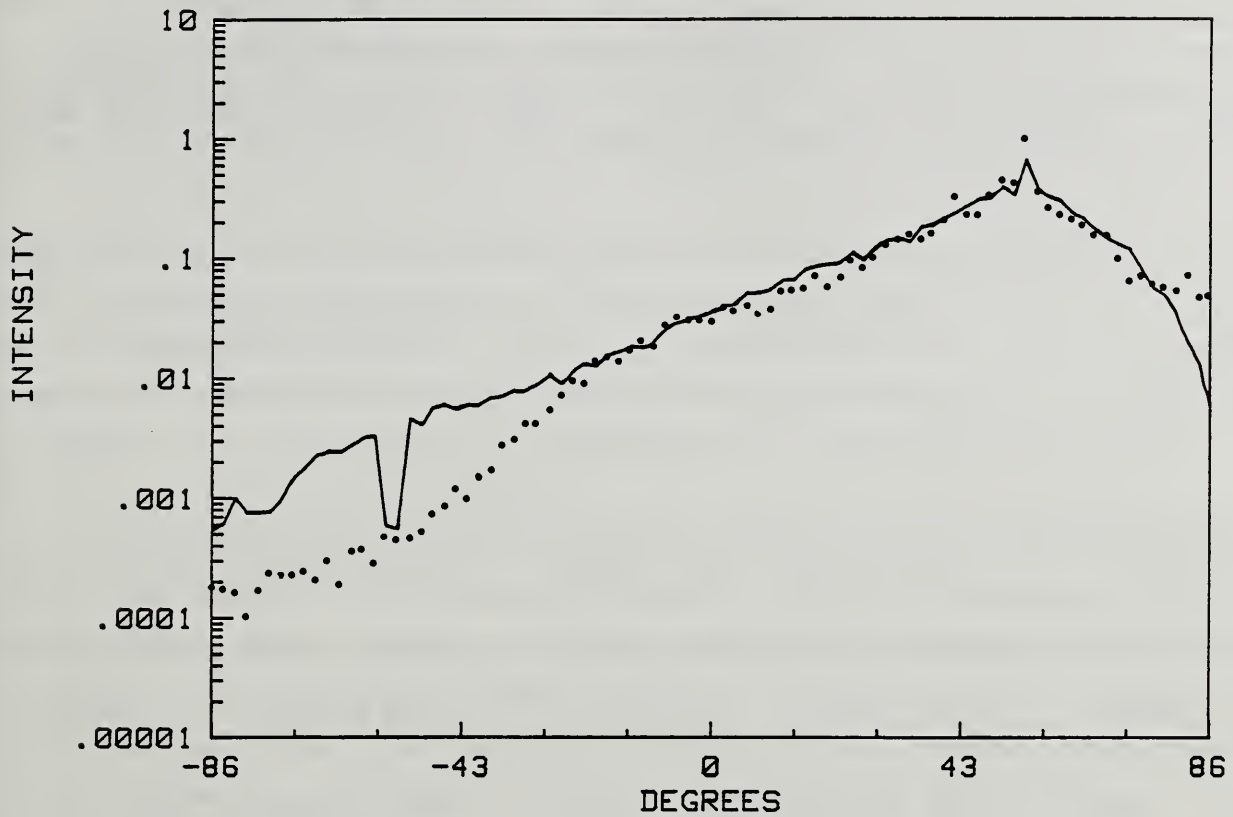


Figure 18 Angular scattering distribution obtained from flat NASA specimen #3 using the DALLAS system. The angle of incidence was -54° . Also shown is the theoretical distribution generated from topographic data measured by a stylus instrument.

TABLE IV

Comparison of stylus and optical measurements of sinusoidal roughness parameters. Uncertainties in the stylus results represent estimates of both random and systematic errors. Uncertainties in the optical results represent estimates of random errors only. For the $R_a = 1\mu\text{m}$, $D = 800\mu\text{m}$, surface the value of $D = 800\mu\text{m}$ was assumed and the corresponding best value of R_a was calculated.

Nominal Surface ($(R_a, D)(\mu\text{m})$)	Parameters Measured by Stylus		Parameters Deduced from Optical Technique	
	R_a (μm)	D (μm)	R_a (μm)	D (μm)
Brass (1, 40)	1.02 ± 0.02	40.1 ± 0.4	1.016 ± 0.002	39.89 ± 0.03
Brass (1, 100)	1.02 ± 0.02	100.2 ± 0.4	1.006 ± 0.003	99.6 ± 0.2
Brass (1, 800)	1.01 ± 0.02	800 ± 11	1.003 ± 0.014	(800)
Nickel (1, 100)	1.03 ± 0.02	100.2 ± 0.4	1.011 ± 0.002	100.2 ± 0.3
Nickel (0.3, 100)	0.31 ± 0.02	100.2 ± 0.4	0.313 ± 0.004	100.8 ± 0.7
Nickel (3, 100)	2.98 ± 0.04	100.1 ± 0.4	2.99 ± 0.05	99.3 ± 1.3

fitting calculation, the best value of R_a was in very good agreement with the results from stylus data.

The close agreement between the optically derived parameters and the stylus results depended on two factors: the validity of the optical scattering theory and the validity of the sinusoidal model of the surface profiles.

The next step in our research will be to develop a suitable statistical model that incorporates appropriate roughness parameters for random surface profiles typical of the NASA hand lapped specimens. Then the combination of this statistical surface model, the optical scattering theory (which so far has proved out to be valid), and mathematical inversion techniques will lead to the measurement of surface roughness parameters from first principles without resorting to comparator approaches.

A promising surface model, developed by Beckmann and Spizzichino [19], uses the rms roughness and the autocorrelation length as parameters. We plan to test whether this two parameter model will adequately characterize the surface statistics of the specimens and then attempt to determine the rms roughness and autocorrelation length from the optical scattering data obtained from DALLAS.

If successful, the models and inversion techniques could then be incorporated into the software of a controller for the MSG, an instrument whose hardware is better suited than DALLAS to on line measurement in manufacturing. Such an instrument will be an important breakthrough for the inspection of surfaces roughness not only for wind tunnel models but other types of manufactured components as well.

6. Acknowledgments

The work described here was largely supported by NASA Contracts L-4618B and L-20078B. Part of the supporting research was supported by the NBS Office of Nondestructive Evaluation and the Navy Materiel and Air and Sea Systems Commands. V. S. Gagne and S. A. Swearingen expertly assisted in the preparation of the manuscript. We also thank J. Zimmerman and E. P. Whitenton for their careful reviewing of the manuscript.

7. References

- [1] E. C. Teague, T. V. Vorburger, F. E. Scire, S. M. Baker, S. W. Jensen, C. Trahan, and B. B. Gloss, "Evaluation of Methods for Characterizing Surface Topography of Models for High Reynolds Number Wind-Tunnels", in AIAA 12th Aerodynamic Testing Conference, Pub. CP-822 (American Institute of Aeronautics and Astronautics, New York, 1982) pp. 246-251.
- [2] E. C. Teague, F. E. Scire, S. M. Baker, and S. W. Jensen, "Three-Dimensional Stylus Profilometry," Wear 83, 1-12 (1982).
- [3] T. V. Vorburger, M. J. McLay, F. E. Scire, D. E. Gilsinn, C. H. W. Giauque, and E. C. Teague, "Surface Roughness Studies for Wing Tunnel Models Used in High Reynolds Number Testing", J. Aircraft 23, 56-61 (1986).
- [4] D. E. Gilsinn, T. V. Vorburger, F. E. Scire, E. C. Teague, and M. J. McLay, "Surface Texture Characterization by Angular Distribution of Scattered Light," in Review of Progress in Quantitative Nondestructive Evaluation, Vol. 4B, D. O. Thompson and D. E. Chimenti, eds. (Plenum, New York 1985) pp 779-788.
- [5] T. V. Vorburger, E. C. Teague, F. E. Scire, M. J. McLay, and D. E. Gilsinn, "Surface Roughness Studies with DALLAS-Detector Array for Laser Light Angular Scattering", J. Res. NBS 89, 3-16 (1984).
- [6] D. E. Gilsinn, T. V. Vorburger, E. C. Teague, M. J. McLay, C. Giauque, and F. E. Scire, "Surface Roughness Metrology by Angular Distributions of Scattered Light", Measurement and Effects of Surface Defects and Quality of Polish, SPIE Vol. 525 (1985) pp 2-15.
- [7] T. V. Vorburger, D. E. Gilsinn, F. E. Scire, M. J. McLay, C. H. W. Giauque, and E. C. Teague, "Optical Measurement of the Roughness of Sinusoidal Surfaces", Wear 109, 15-27 (1986).
- [8] D. Gilsinn, T. Vorburger, L. X. Cao, C. Giauque, F. Scire, and E. C. Teague, "Optical Roughness Measurement of Industrial Surfaces", in Optical Techniques for Industrial Inspection, SPIE Vol. 665 (1986) pp. 8-16.
- [9] N. Schlichting, Boundary Layer Theory, 7th edition, translated by J. Kestin (McGraw Hill, New York, 1979).
- [10] R. Brodmann, O. Gerstorfer, and G. Thurn, "Optical Roughness Measuring Instrument for Fine-Machined Surface", Opt. Eng. 24, 408-413 (1985).
- [11] ANSI/ASME B46.1-1985, Surface Texture (Surface Roughness, Waviness and Lay) (American Society of Mechanical Engineers, New York).
- [12] D. V. Huntsberger and P. Billingsley, Elements of Statistical Inference, Third Ed. (Allyn and Bacon, Boston, 1973), p. 227.

- [13] N. R. Draper and H. Smith, Applied Regression Analysis (John Wiley and Sons, New York, 1960).
- [14] See for example, P. R. Bevington, Data Reduction and Error Analysis for the Physical Sciences (McGraw-Hill, New York, 1969), p. 196.
- [15] S. T. Peavy, R. N. Varner, and D. Hogben, Source Listing of OMNITAB II Program, NBS Special Publication 339 (U. S. Dept. of Commerce, Washington, DC, 1970).
- [16] R. S. Sayles in Rough Surfaces, T. R. Thomas, ed., (Longman, London, 1982) Chapter 5.
- [17] L. W. McKinney, "Overview of National Transonic Facility Model Technology Program", in Cryogenic Wind Tunnel Models, Design and Fabrication, C.P. Young, Jr. and B.B. Gloss, eds.. NASA CP 2262, pp. 1-9.
- [18] Navy Manufacturing Technology Program Report, (Naval Material Command Industrial Resources Detachment, Philadelphia) August, 1985, p. 6.
- [19] P. Beckmann and A. Spizzichino, The Scattering of Electromagnetic Waves from Rough Surfaces (Pergamon, Oxford, 1963).

APPENDIX A

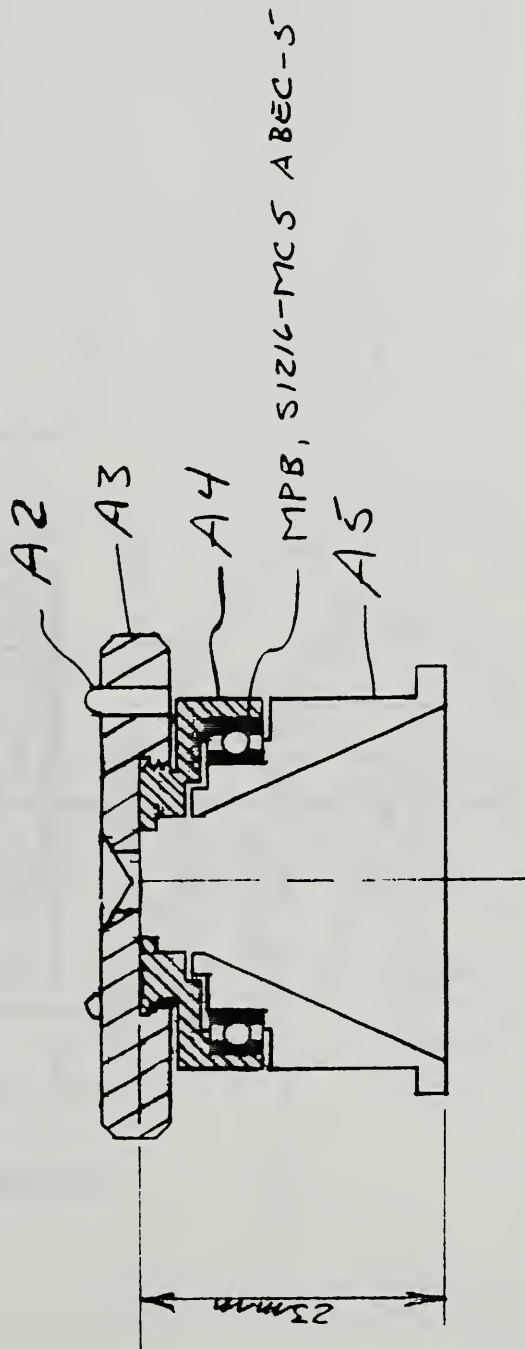
Shop drawings on the most recent MSG nosepiece fabricated at NBS. The design is still evolving so a few of these dimensions may be slightly different from those of previous manifestations. We use a precision bearing to allow z-rotation but also to minimize the degree of wobble about the x- and y-axes (see Fig. 3).

NOTE:

1) MAT'L:

PIECES A4 & A5
BLACK ANODIZED
ALUM 2024-T6

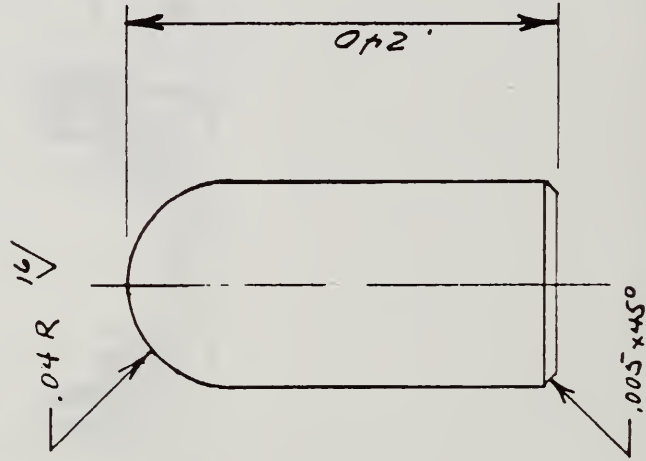
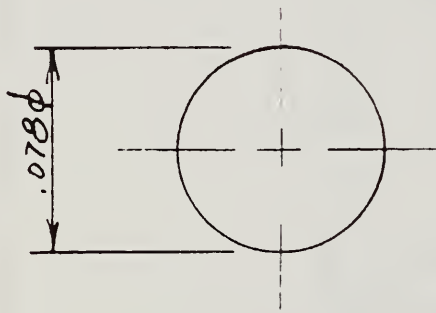
PIECES A2 & A3
BLACK DELRIN



NATIONAL BUREAU OF STANDARDS WASHINGTON, D.C. 20234	
DRAFTSMAN FES	DATE 3/9/87
DIVISION 737	SCALE 2/1
ASSY A1	

NOTES:

- 1.) Mat'l: Black Delem
- 2.) DIM. T. 0.05
- 3.) 3 Pieces Redd.
- 4.) PINS TO BE PRESS FIT WITH PARTS



NATIONAL BUREAU OF STANDARDS
WASHINGTON, D.C. 20234

DRAFTSMAN Fes	DATE 3/9/87	SCALE N/S	NOSE PIECE PINS
DIVISION 737	AZ		

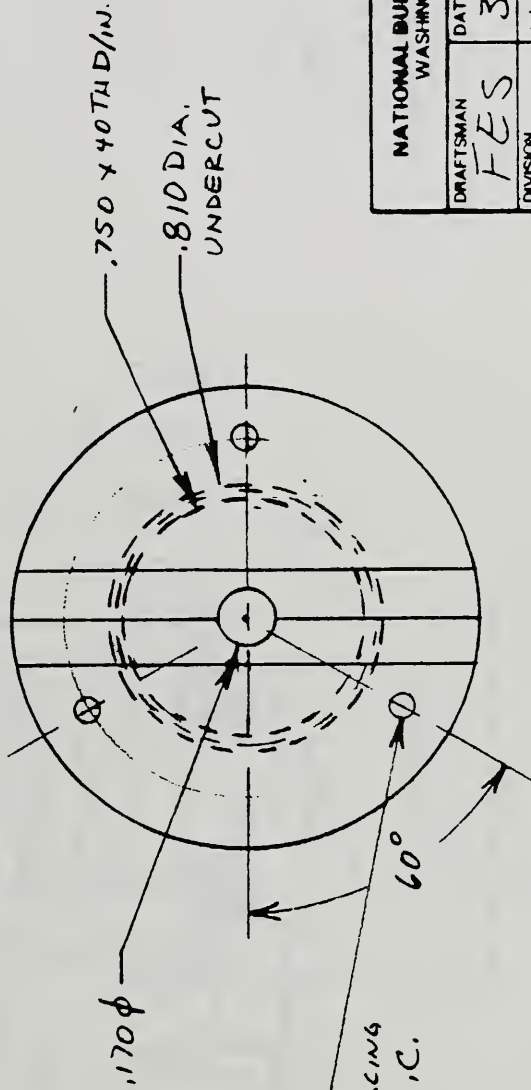
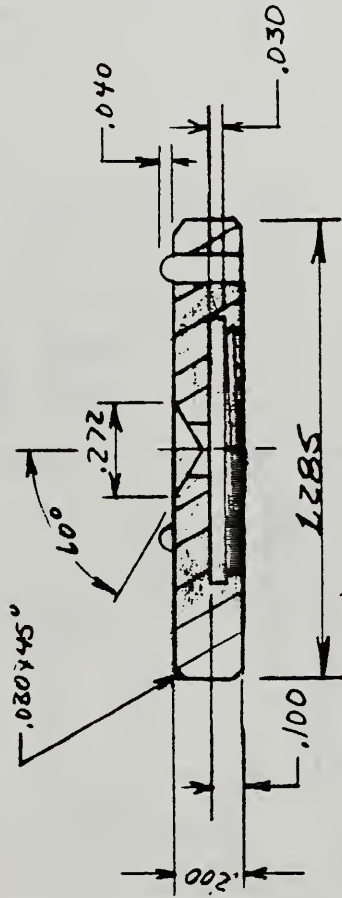
NOTES:

1) MAT'L: BLACK DELRIN
BODY & 3 PINS

2.) TOLERANCES $\pm .005$

UNLESS NOTED

3) BREAK ALL EDGES
 $.005 \times 45^\circ$

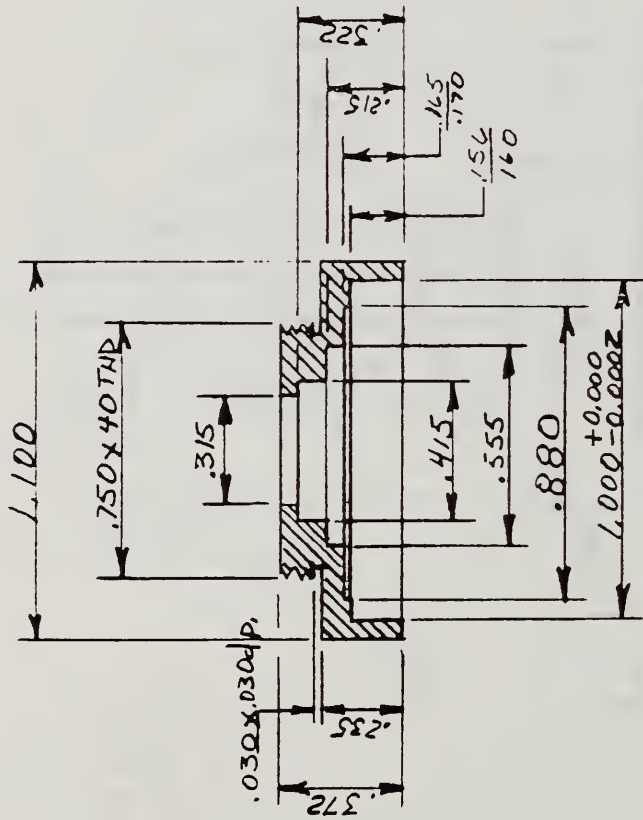


$.078 \phi$ PINS
3 POS @ 120° SPACING
ON 1.047ϕ B.C.
16/

NATIONAL BUREAU OF STANDARDS WASHINGTON, D.C. 20234			
DRAFTSMAN FES	DATE 3/9/87	SCALE 2/1	
DIVISION 737	NOSE PIECE ✓/PINS		A3

NOTES:

- 1) MAT'L - ALUM ALLOY 2024
BLACK ANODIZE
- 2) 1.00 DIA. IS PRESS FIT
FOR SUPPLIED BEARING
- 3) TOLERANCES $\pm .005$
UNLESS NOTED
- 4) BREAK ALL EDGES
1005 X 450



NATIONAL BUREAU OF STANDARDS WASHINGTON, D. C. 20234			
DRAFTSMAN FES	DATE 3/9/87	SCALE 2/1	
DIVISION 737	NO. OF PIECE ADAPTER		A4

U.S. DEPT. OF COMM. BIBLIOGRAPHIC DATA SHEET (See instructions)		1. PUBLICATION OR REPORT NO. NBSIR 87-3586	2. Performing Organ. Report No.	3. Publication Date July 1987
4. TITLE AND SUBTITLE THE WIND TUNNEL MODEL SURFACE GAUGE FOR MEASURING ROUGHNESS				
5. AUTHOR(S) T.V. Vorburger, D.E. Gilsinn, E.C. Teague, C.H.W. Giauque, F.E. Scire, and L.X. Cao				
6. PERFORMING ORGANIZATION (If joint or other than NBS, see instructions) NATIONAL BUREAU OF STANDARDS U.S. DEPARTMENT OF COMMERCE GAITHERSBURG, MD 20899			7. Contract/Grant No. L4718B and L20078B	8. Type of Report & Period Covered Final
9. SPONSORING ORGANIZATION NAME AND COMPLETE ADDRESS (Street, City, State, ZIP) NASA Langley Research Center Hampton, VA 23665				
10. SUPPLEMENTARY NOTES <input type="checkbox"/> Document describes a computer program; SF-185, FIPS Software Summary, is attached.				
11. ABSTRACT (A 200-word or less factual summary of most significant information. If document includes a significant bibliography or literature survey, mention it here) This report covers research performed in the optical inspection of surface roughness by members of the Center for Manufacturing Engineering under contracts L-4718B and L-20078B with the NASA Langley Research Center. The project has proceeded along two lines: first, research into a quantitative understanding of light scattering from metal surfaces and into the appropriate models to describe the surfaces themselves, and second, the development of a practical instrument for the measurement of rms roughness of high performance wind tunnel models with smooth finishes. The research has been discussed in previous articles and is only summarized here. This report is concerned primarily with the latter subject. We have developed a practical technique for the optical estimation of rms roughness based on three things: a commercially available, optical roughness gauge, a special nosepiece that allows for rapid alignment of the gauge on curved surfaces, and a series of comparator studies that correlate the results for S_N obtained by the gauge with rms roughness (R_a) measurements of surfaces by stylus techniques. S_N is an optical scattering parameter that is proportional to the variance of the light scattering angular distribution about its mean angle. We have proposed upper limit criteria for the value of S_N that should be expected on a properly finished model surface having rms roughness less than $0.2\mu\text{m}$. We have estimated that valid measurements of S_N may be taken within an angle of 60° from the leading edge of the wind tunnel model wing that we tested and have shown from stylus measurements that the roughness increases dramatically around the leading edge				
12. KEY WORDS (Six to twelve entries; alphabetical order; capitalize only proper names; and separate key words by semicolons) aircraft, finish, light scattering, model, optical roughness, optical scattering, rms roughness, roughness, stylus, surface, transonic, wind tunnel				
13. AVAILABILITY <input checked="" type="checkbox"/> Unlimited <input type="checkbox"/> For Official Distribution. Do Not Release to NTIS <input type="checkbox"/> Order From Superintendent of Documents, U.S. Government Printing Office, Washington, D.C. 20402. <input type="checkbox"/> Order From National Technical Information Service (NTIS), Springfield, VA. 22161			14. NO. OF PRINTED PAGES 56	
			15. Price \$13.95	

